AN ABSTRACT OF THE THESIS OF

Joachim Herpe for the degree of Master of Science

in Physics presented on July 17, 1986 .

Title: X-Ray Study of an Isobranched Lecithin

Redacted for privacy

Abstract approved: _____

David J. Griffiths

Lipids, especially phospholipids, are very common but important molecules found in cells and animal tissue, performing many biological functions, particularly in membranes. Lipids, when mixed with water, spontaneously form ordered systems, such as micelles, vesicles and multibilayers. The size of these systems and their degree of ordering depend on the temperature and water content of the sample.

One member of this most important class of molecules is 14-di-isoacyl-phosphatidyl-choline (14 iPC), a modified lipid. The goal of this study was to determine, via X-ray diffraction, the thermotropic phase behavior of bilayers formed by 14 iPC in excess water.

In addition, the projected electron charge density perpendicular to the plane of the bilayer was deduced from Fourier transforms of the low-angle X-ray diffraction patterns. An investigation of the stacking disorder of bilayers was conducted by proposing models and comparing their predicted X-ray diffraction patterns with the observed data.

X-Ray Study of an Isobranched Lecithin

by

Joachim Herpe

A THESIS

submitted to

Oregon State University

in partial fulfillment of
the requirements for the
degree of

Master of Science

Completed July 17, 1986

Commencement June 1987

APPROVED:

Redacted for privacy

Professor of Physics in charge of major

Redacted for privacy

Chairman of Department of Physics

Redacted for privacy

Dean of Graduate School

Date thesis is presented July 17, 1986

Acknowledgement

I wish to express my gratitude to Dr. David J. Griffiths, who proposed this study and was of great support in all stages of the process. It was a pleasure for me to work for him.

I also owe my thanks to Dr. H. Hollis Wickman, who kindly provided the X-ray-apparatus and contributed with many helpful discussions to the completion of this work.

Thanks also to Sarah E. Church, who supplied the samples and detectors used in this study and gave considerable moral support.

Special thanks are due to my parents back in Germany, who gave me the financial support and, without really knowing what I was doing, the encouragement that made this work at all possible.

TABLE OF CONTENTS

	Page
INTRODUCTION	1
LIPIDS	3
General form	3
14 iPC	4
Lipid-water systems	7
X-RAY DIFFRACTION	12
Geometry of diffraction	12
Fourier Transform	14
Limiting sphere	16
Determining the electron charge density	18
Disordered systems	22
Concrete model for disordered multilayer	24
APPARATUS	28
RESULTS AND DISCUSSION	34
Phase behavior	34
Electron density models	51
Comparison to DSC results	54
CONCLUSION	56
BIBLIOGRAPHY	59
APPENDIX	62

LIST OF FIGURES

Figure		Page
1.	Chemical formula of 14 iPC	6
2.	Lipids in water forming a micelle	7
3.	Lipids building a bilayer	8
4.	Lipids forming a vesicle	9
5.	Characteristis dimensions of MLVs	10
6.	Lipids in a membrane	11
7.	Bragg-reflection between netplanes	13
8.	Limiting sphere and Ewald sphere	16
9.	Interference function for disorder of the second kind	26
10.	Set-up for X-ray measurements	29
11.	Wide angle calibration spectrum	31
12.	Counts along the detectors in 5mm steps	33
13.	Continuous detector response	33
14.	$L_{\beta'}$ to $P_{\beta'}$ transition of 14 iPC (low angle data)	35
15.	$L_{\beta'}$ to $P_{\beta'}$ transition of 14 iPC (wide angle data)	36
16.	Characteristis dimensions of 14 iPC bilayers	37
17.	Gel-liquid crystal transition of 14 iPC (low angle data)	39
18.	Gel-liquid crystal transition of 14 iPC (wide angle data)	40
19.	High temperature behavior of 14 iPC	42

Figure		Page
20.	Cooling below gel-liquid crystal transition (low angle data)	43
21.	Cooling below gel-liquid crystal transition (wide angle data)	44
22.	Stability of intermediate phase (low angla data)	46
23.	Stability of intermediate phase (wide angle data)	47
24.	Back-transition into $L_{\beta'}$ phase (low angle data)	48
25.	Back-transition into $L_{\beta'}$ phase (wide angle data)	49
26.	Structured wide angle spectrum (-12°C)	50
27.	Model electron density distribution of one bilayer	52
28.	Diffraction pattern of the bilayer	52
29.	Diffraction pattern of 10 disordered bilayers	53
30.	Transition temperatures for 14 iPC and DPPC	57
31.	Lamellar structures of 14 iPC	57

X-Ray Study of an Isobranched Lecithin

INTRODUCTION

Lipids are very common constituents in cells and animal tissue. They are macromolecules with a polar head and a nonpolar tail. This makes them useful for different biological functions, especially in membranes. About 50% of the lipids in cells and tissues are phospholipids. The most common representative of this group is phosphatidylcholine (lecithin), found in almost any kind of cell-material. One member of this family is 14-di-isoacyl-phosphatidyl-choline (14 iPC).

All lipids form ordered systems when they come in contact with water. Since their polar headgroup is hydrophilic and the non-polar tail hydrophobic, they arrange themselves in systems, in which the tailgroups (hydrocarbon chains) are sheltered from the water. They build up closed systems such as micelles and vesicles,

which have selfsealing properties like natural membranes.

The arrangement of 14 iPC in excess water was studied here using X-ray diffraction in both the small-angle region, in which we determine the repeat distance of these bilayers, and the wide angle region, which gives information about the ordering of the hydrocarbon chains. From the X-ray diffraction pattern the electron charge density along the axis normal to the bilayer plane was determined. Since for this procedure the scattering function has to be known, but only its absolute square is measured, we are left with the problem of determining the phase factor. Fortunately, in the case of 14 iPC, the electron density is centro-symmetric and, therefore, this phase factor is +1 or -1, corresponding to phase angles of 0 and π, respectively.

To determine the correct electron charge density function for the bilayer, models of it were made and their expected X-ray diffraction patterns were compared to the observed data. Finally, the results were compared with those from DSC-measurements (Lewis/ McElhaney, 1985).

LIPIDS

General form

Lipids are water-insoluble organic biomolecules, which are found in cells and animal tissue of any kind (e.g. myelin, a substance found in nerve fibers, is composed of up to 80% lipids). They have the following important biological functions:

- as structural components of membranes,
- as a protective coating on the surface of many organisms,
- for storage and transport of metabolic fuel,
- as cell-surface components responsible for cell recognition, species specificity and tissue immunity.

Lipids often appear combined with other biomolecules, to which they are either weakly or covalently bonded. This way they build hybrid-molecules such as glyco-lipids and lipoproteins.

In general one distinguishes two large classes of lipids:

The so-called complex lipids like acylglycerols and phosphoglycerides contain (usually two) fatty acids and are, therefore, saponifiable (i.e. they can form a soap). In natural membranes, the lipids contain usually two different fatty acids (e.g. a saturated and an unsaturated one) while in model membranes (formed in a lab) they contain identical acids. To this group belong, for example, all the waxes.

The other group consists of the simple lipids, which do not contain fatty acids and, therefore, are also not saponifiable. This class includes among others the vitamins and hormones.

14 iPC

Very common among the complex lipids are the phosphoglycerides, often simply (but not quite correctly) called phospholipids. In fact they make up about 50% of

all lipids found in cell tissue. The most common of these is phosphatidylcholine, better known as lecithin. This substance is found in almost any tissue,such as, the liver, blood plasma, eggs, and the brain substance.

The subject of the following work was a molecule called 14-di-isoacyl-phosphatidyl-choline (14 iPC). Its chemical configuration is shown in figure 1.

14 iPC consists of a polar headgroup, containing the PC-part, and a non-polar tail, build up of the two hydrocarbon chains, being isobranched in this case (i.e. the chains are split after the 13th methylgroup. Thus, there are 15 methylgroups in a chain which is still only 14 "carbons" long). The most important feature of the headgroup is that it is hydrophilic, i.e. it has a tendency to attract water molecules. In contrast, the tail is hydrophobic, i.e. it tries to avoid contact with water molecules. The molecule is not as rigid as most inorganic molecules, but is able, e.g., to twist its hydrocarbon chains, and to bend the headgroup to different orientations. Thus, for the dimensions, only approximate values can be given. The headgroup is of the order of seven angstroems (7Å) long, while the tail has a length of about 15 angstroems (15Å).

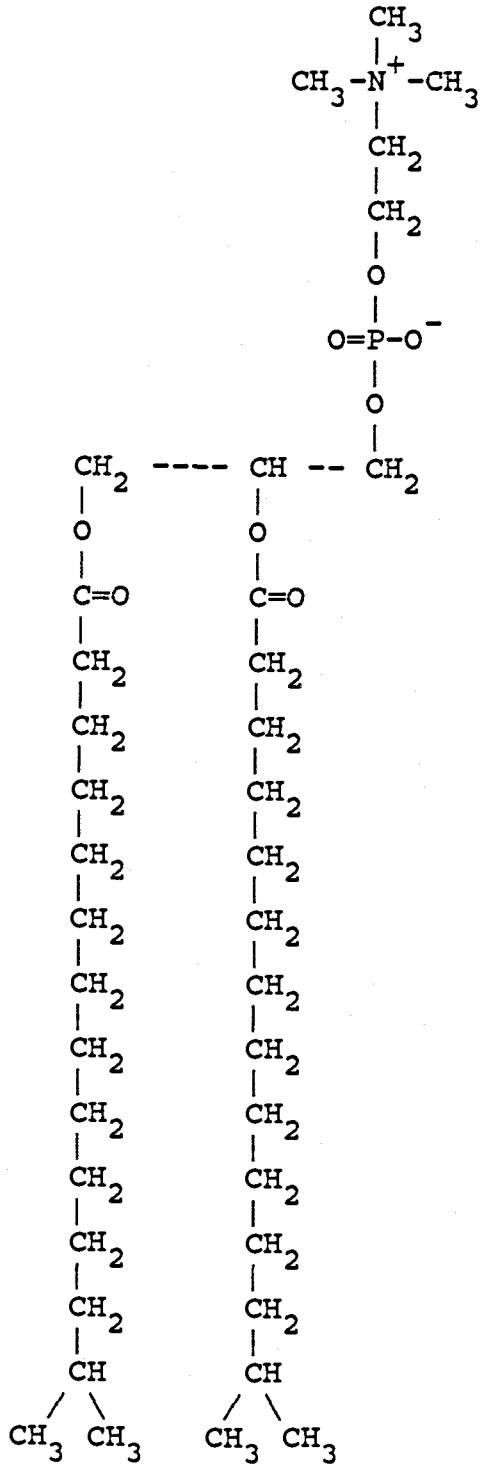

Fig. 1: Chemical formula of 14 iPC.

Lipid-water-systems

When lipids are dispersed in water, they spontaneously form stable structures. Also at the air-water interface they build up monolayers, with the polar headgroups in the water and the non-polar tails in the air region. There are several ways lipids arrange themselves in water. At low concentrations they build micelles (see Fig. 2), where there is a group of lipids with the heads at the outside and the tails inside, such that the tails are sealed from the water.

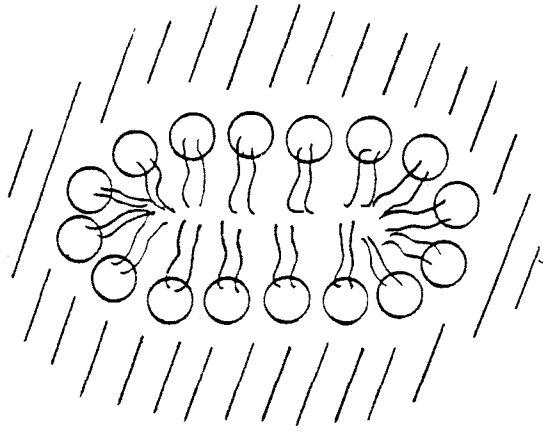

Fig. 2: Lipids in water forming a micelle.

If such a micelle gets bigger, a bilayer evolves, in which the lipid-molecules form a plane, with the heads at the surfaces of it and the tails in the center (see Fig. 3).

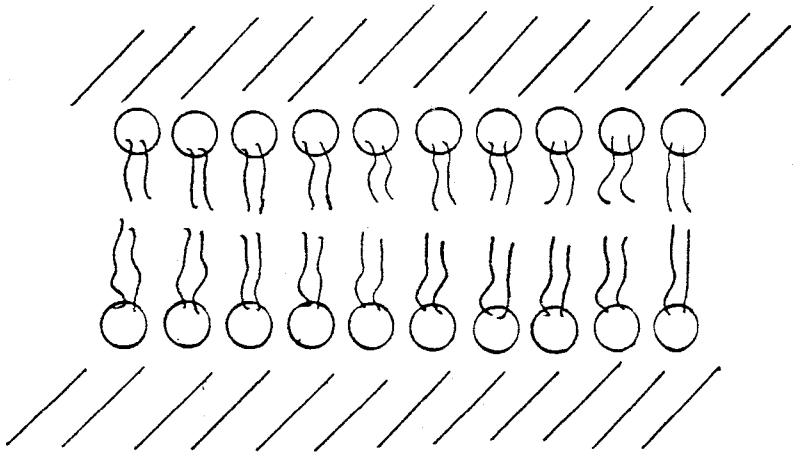

Fig. 3: Lipids building a bilayer.

These bilayers do not have to be planar objects, but can also constitute (spherical) shells, with water at the center, then a lipid bilayer, then again water (see Fig. 4). These aggregates are then called vesicles. This is one way bilayers are established in lipid-water-systems, besides the stacking similar to a (smectic D) liquid crystal. The vesicles have self-sealing properties like natural membranes.

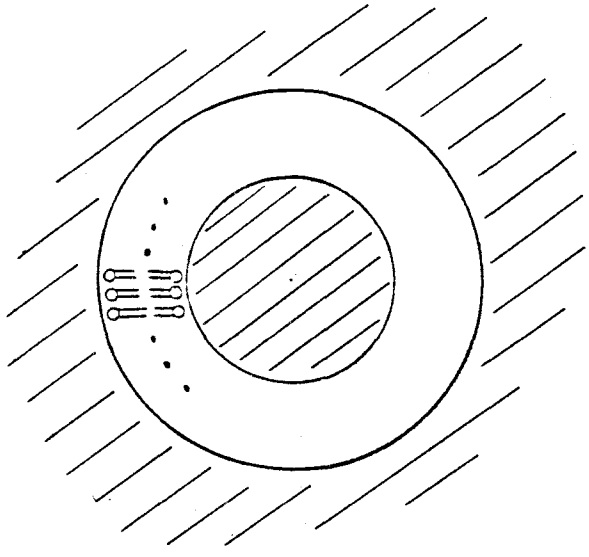

Fig. 4: Lipids forming a vesicle.

The type of sample geometry we worked with in this study consists of several layers of vesicles around each other, like shells in an onion. These aggregates are called multilamellar vesicles (MLVs, see Fig. 5). The size of these MLVs and the repeat distance of their layers is characteristic for the phase they make up. They depend on the temperature and the degree of hydration of the sample. Representative values are some 40 to 70 Å for the repeat distance d, and about 400 up

to 1000 Å for their radius R.

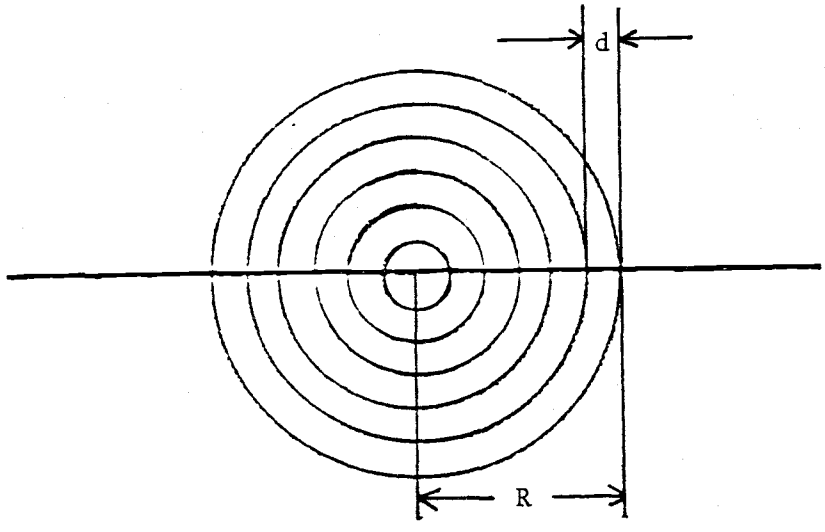

Fig. 5: Characteristic dimensions of MLVs.

These properties of lipids are used in building up biological membranes, for which properties like elasticity and selective permeability are important. In membranes, lipids form a bilayer, which is coated at the surfaces with a layer of proteins (see Fig. 6).

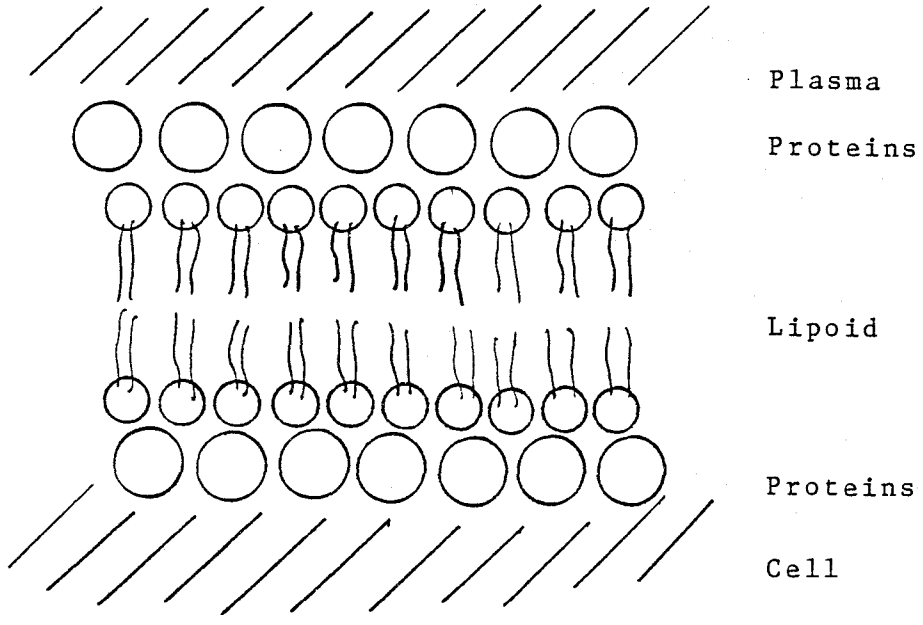

Fig. 6: Lipids in a membrane.

Lipids are, however, not only present in the cell-surfaces, but also in sub-cellular components like mitochondria.

X-RAY DIFFRACTION

Geometry of diffraction

X-rays are scattered by electrons present in material. Therefore, the amplitude of the scattered wave is directly proportional to the local electron density. For a dilute system of scatterers far from resonance absorption, X-rays are scattered elastically, which means that the incoming and outgoing wave-vectors have the same modulus. It is usually taken to be $1/\lambda$. The scattering is characterized by the difference S between the incoming (S_0) and outgoing (S') wave-vector (see Fig. 7).

From trigonometry we get then the modulus of S:

$$|S| = S = 2\sin\theta/\lambda, \qquad (1)$$

where 2θ is the scattering angle. Because of the Bragg-condition, $\sin\theta$ is directly proportional to λ,

$$n\lambda = 2d\sin\theta, \qquad (2)$$

where d is the distance between the "reflecting" netplanes. Therefore S is independent of the wavelength of the used radiation. Braggs condition is satisfied if S corresponds to certain values defined by

$$S = n/d. \qquad (3)$$

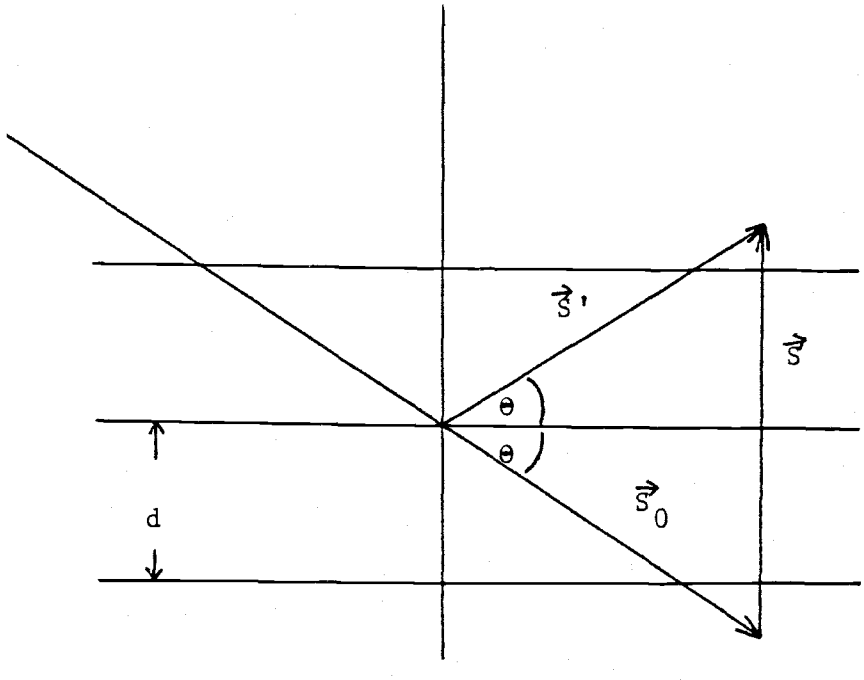

Fig. 7: Bragg-reflection on netplanes.

These values determine the reciprocal lattice points at which the scattered wave has non-zero value. For a three dimensional lattice in real space we get these conditions also for three components for the vector S. Thus the endpoints of S will lie on a three dimensional lattice, with lattice vectors having the unit 1/length, and therefore are called reciprocal lattice vectors. Each of these is perpendicular to its corresponding real lattice vector, since the parallel vector S is always normal to the netplanes on which the scattering occurs.

Fourier Transform

The wave scattered in direction r relative to the origin has the form

$$f = f_0 \exp[i2\pi(\vec{S}\cdot\vec{r} + a)] \qquad (4)$$

where f_0 is the scattering strength of the atom and "a" is a phase factor.

The resultant wave scattered by the entire array of atoms in the sample is then

$$F(\vec{S}) = \int_{-\infty}^{\infty} \rho(\vec{r}) \exp[2\pi i(\vec{S}\cdot\vec{r} + a)] \, dV, \qquad (5)$$

where the integration goes over the entire sample volume. The electron charge density $\rho(\vec{r})$ of the entire sample (say, a crystal) is a function of the electron density of the unitcell and the arrangement of all unitcells in the sample. It can be expressed as

f(crystal) =

f(unitcell) * [f(infinite lattice) x f(shape)] (6)

Here "*" means a convolution (see Goodman, 1968) and "x" a multiplication. This leads then to the Fourier-transform

T[f(crystal)] = T[f(unitcell)] x

{T[f(infinite lattice)] * T[f(shape)]} (7)

$F(\vec{S})$ is the Fourier transform of this electron charge density of the sample and is called scattering amplitude or structure factor. While it is defined over

all reciprocal space, only part of this function can be obtained by measuring the scattered wave.

Limiting sphere

As seen in eq.1, the modulus (and thus length) of the vector S is at most $2/\lambda$. Thus only that part of the Fourier transform that lies in a sphere of radius $2/\lambda$ around the origin of reciprocal space (the endpoint of the vector S_0) can be observed (see Fig. 8).

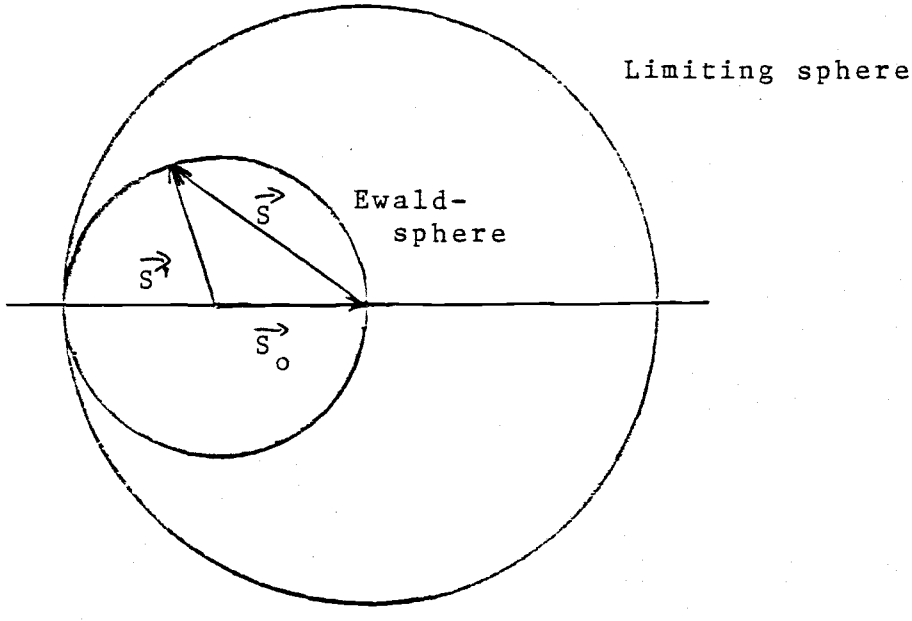

Fig. 8: Limiting sphere and Ewald sphere.

The endpoint of the vector S lies always on a sphere around the origin of vector S_0 with radius $1/\lambda$. This sphere is called Ewald sphere. Only at points of the reciprocal lattice which lie on this sphere will the X-ray diffraction pattern have non-zero intensity. Thus, it may be necessary to rotate the sample in order to get a diffraction pattern at all, or to extract all the information contained in the limiting sphere. If the sample is of powder form (like our MLVs in aqueous dispersion) instead of crystallite form, non-zero condition is intersection of a sphere of radius S with the Ewald sphere instead of discrete points only, i.e. a circle on the Ewald sphere. Therefore, the diffracted X-radiation has the shape of cones, leaving on a screen perpendicular to the direct beam concentric circles.

Since in order to discover finer details, a large portion of the Fourier transform has to be known, the wavelength of the X-radiation, which determines the radius of the limiting sphere, should be chosen as small as possible. Practical considerations limit this choice to a few wavelengths when using conventional X-ray sources (using synchrotron radiation improves the situation considerably).

Determining the electron charge density

To determine the electron charge density from the measured X-ray diffraction pattern we need the amplitude and phase of the scattering function, from which we can then calculate the electron charge density by using the inverse Fourier transform on that function. Yet we can only measure the intensity of the scattered wave,

$$I(S) = F(S)F^{*}(S) \qquad (8)$$

and that only at certain points in reciprocal space. Fortunately, the electron charge density in the unit cell is centrosymmetric, as can easily be concluded from the configuration of the bilayers, and, therefore, the phase factors are either +1 or -1. This leaves us with 2^n possible variations of the phase factors for n observed orders of diffraction.

$$F(S) = \pm[I(S)]^{1/2} \qquad (9)$$

Knowing F(S) we can calculate the electron charge

density $\rho(\vec{r})$ from

$$\rho(\vec{r}) = \int_{-\infty}^{\infty} F(\vec{S}) \exp[-2\pi i \vec{S}\cdot\vec{r}]\, dV' \qquad (10)$$

where the integration is over the entire reciprocal space.

For a planar array with N planes and a repeat distance d the electron charge density is periodic

$$\rho(x,y,z) = \rho(x+nd,y,z). \qquad (11)$$

The scattering function is then

$$F(\vec{S}) = \int_{-\infty}^{\infty}\int_{-\infty}^{\infty}\int_{0}^{Nd} \rho(x,y,z) \exp[2\pi i(S_x x+S_y y+S_z z)]\,dx\,dy\,dz \qquad (12)$$

Integration over both y and z dependences yields a kind of projection of $\rho(x,y,z)$, say $\bar{\rho}(x)$,

$$\bar{\rho}(x) = \int_{-\infty}^{\infty}\int_{-\infty}^{\infty} \rho(x,y,z) \exp[2\pi i(S_y y+S_z z)]\,dy\,dz \qquad (13)$$

so that $F(\vec{S})$ is reduced to a one dimensional function along one axis of reciprocal space.

$$F(S) = \int_0^{Nd} \bar{\rho}(x) \exp[2\pi i S_x x] dx \qquad (14)$$

Since $\bar{\rho}(x)$ is periodic, the integral over the entire sample can be reduced to the integral over one unit cell and a sum

$$F(S) = F_u(S) \sum_{n=1}^{N-1} \exp[2\pi i S n d] \qquad (15)$$

with

$$F_u(S) = \int_{-d/2}^{d/2} \bar{\rho}(x) \exp[2\pi i S x] dx \qquad (16)$$

$F_u(S)$ is the structure factor of a single diffraction unit. From it the electron charge density can be deduced by the inverse Fourier transform operation

$$\bar{\rho}(x) = \int_{-\infty}^{\infty} F_u(S) \exp[-2\pi i S x] dS \qquad (17)$$

The periodicity of $\bar{\rho}(x)$ allows one to convert the integral into a sum

$$\bar{\rho}(x) = b(0)/d + 2/d \sum_{h=0}^{\infty} F_u(h/d)\cos(2\pi hx/d) \qquad (18)$$

The constant term b(0)/d can not be determined, since it corresponds to scattering at angle zero, which is on the axis of the direct beam (and thus usually strikes a beam stop). It is undefined and gives the background charge density. The other terms on the right-hand side of eq. (16) determine the deviation of the electron charge density about this value, i.e. $\bar{\rho}(x)$ is a contrast function with both positive and negative values. Usually the reference level is the electron charge density of water, which is 0.334e/A .

The terms b(h) with

$$b(h) = F_u(h/d)\cos(2\pi hx/d) \qquad (19)$$

are known only for a few orders, which means that the Fourier series has to be truncated. This usually causes some trouble. Therefore, the most reliable method of determining the electron charge density along the bilayer axis is to make a model and to compare the Fourier transform of the model's electron charge density with the observed diffraction pattern.

Disordered systems

A commonly observed diffraction effect is for the Bragg reflections to become wider, the larger the diffraction angle. The widths of the reflections can be increased by instrumental broadening, resulting e.g. from the finite width of the X-ray beam, the finite thickness of the sample, as well as a lack of monochromaticity.

If the broadening is larger than that calculated for instrumental effects, then a variation in the repeat distance is indicated. It can be that this distance varies from stack to stack in a specimen, but also that the distance varies from one membrane to another within a stack. A likely site for variability is in the spaces between membranes. It can vary both along the membrane surface and in the direction normal to the surfaces. In general the thickness will vary if the spaces are filled with water and there are no direct contacts between membranes, since the water molecules will have liquid-like disorder. If the spaces between layers are determined by direct contact, then

the spaces will vary since the contacts will be irregular. Also, the repeat distance will vary with time at each point in a membrane (dynamic stacking disorder), resulting from the lateral diffusion of the molecules. Finally, molecules can move in and out of the bilayer, making the bilayer structure fluctuate from instant to instant.

The spaces between membranes vary and the variations do not correlate from one space to the next. Therefore, the repeat distance varies randomly from one membrane to another in a stack (random stacking disorder). Each succeeding membrane will be placed in relation to the actual position of the next nearest neighbor, thus eliminating a definite long range order (disorder of the second kind), rather than in relation to an ideal equilibrium position with long range order among the molecules (disorder of the first kind, mainly from thermal motion). A stack having disorder of the second kind is described as showing short-range order. The uncertainty in the distance between two membranes separated by many others in a stack will grow with the numbers of intervening membranes.

This disorder of the second kind is the one plausible for multilayers or membranes, since disorder of the first kind requires contraints that are absent here.

Concrete model for a disordered multilayer

To build a concrete model for a disordered multilayer, first a pair-correlation function h(x) has to be defined, which is a histogram of possible distances between different pairs of neighbouring membranes. It is possible to predict the diffraction from the pair-correlation function.

An alternative approach is to Fourier transform the diffracted intensity, taking the phase angles to be zero. The result is an auto-correlation function (Patterson function). It is a histogram of all the distances between membranes in the multilayer.

For disorder of the second kind the squared Fourier transform of the model multilayer is

$$|F(S)|^2 = |F_o(S)|^2 \times \{N + 2\sum_{n=1}^{N-1}(N-n)H^n(S)\cos(2\pi nSd)\} \qquad (20)$$

where the term in curly brackets is called interference function (Blaurock, 1982), and H(S) is defined as

$$H(S) = \int_{-\infty}^{\infty} h(x)\exp[-2\pi ixS)dx \qquad (21)$$

thus being the Fourier transform of the pair-correlation function. $F_o(S)$ is the Fourier transform of the single membrane profile

$$F_o(S) = \int_{-d/2}^{d/2} \bar{\rho}(x)\exp[2\pi ixS]dx \; . \qquad (22)$$

In the case of no disorder H(S) would be equal to unity (h(x) being a Dirac delta-function). With increasing disorder the distances between the bilayer-centers will be distributed around a mean value d. This can be regarded as broadening and decreasing the peak of the delta function, e.g. yielding a Gaussian function, the Fourier transform of which is again a Gaussian.

From eq.(20) we can generate the interference

function I(S) for disorder of the second kind, being

$$I(S) = |F(S)|^2/|F_o(S)|^2 \qquad (23)$$

(see Fig. 9). Instead of having a comb-function like for a perfect crystal, the intensity in the peaks will fall while the background will rise with increasing scattering angle. The complete scattering of multi-bilayers is then given by the diffraction pattern of one unitcell multiplied with the appropriate interference function.

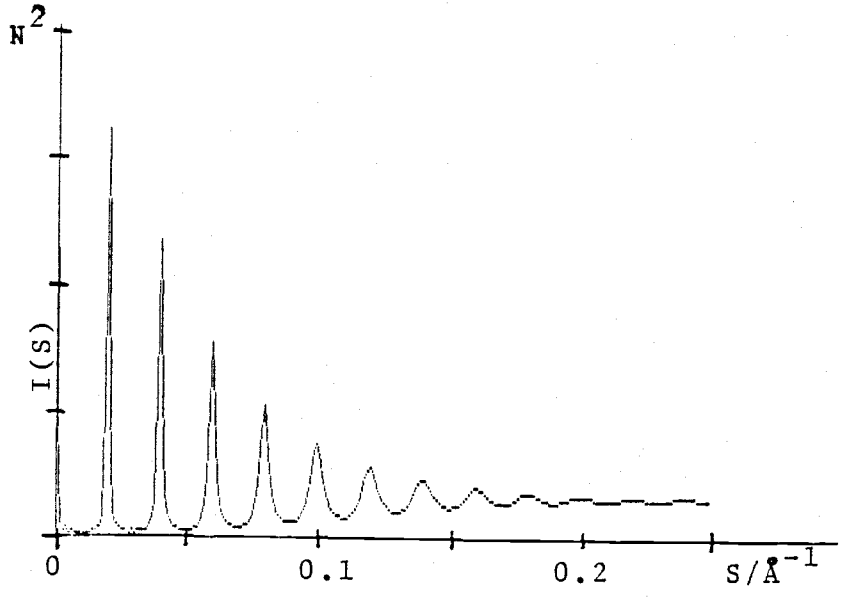

Fig. 9: Interference function for disorder of the second kind.

At large angles the diffraction will be as from N entirely independent point-scatterers. The greater the disorder, the wider will h(x) be and therefore the narrower H(S), i.e. the more rapidly will the intensity of the peaks go down. If the width of the Bragg peaks in the observed diffraction pattern increases with increasing diffraction angle, then disorder of the second kind is indicated.

APPARATUS

The X-ray scattering was done with a Phillips X-ray tube, using a copper target. The wavelength of the radiation was 1.5418E-10 m, known as K-alpha radiation. The tube was operated at a voltage of 37 kV and a current of 25 A. The collimated beam hit the sample housed in a special cage, and the scattered beam was observed with two position sensitive detectors. The sample was sealed in a glass tube of 1.00 mm diameter with a wall thickness of 0.01 mm.

To reduce disturbing scattering effects from air the sample cage and the space between the sample cage and the detectors received a special atmosphere from a steady flow of helium gas. The position sensitive detectors were operated at a voltage of 2600 V. Therefore, they had to be in an atmosphere of P10-gas (a mixture of about 10% Methane and 90% Argon), to prevent electrical discharge. The pulses received at these detectors were processed by a set of delay-amplifiers and the data were stored in two ND 62 (Nuclear Data Co.) multichannel-analyzers (see

Fig. 10). The data were then transferred to a PDP-11 computer to be processed.

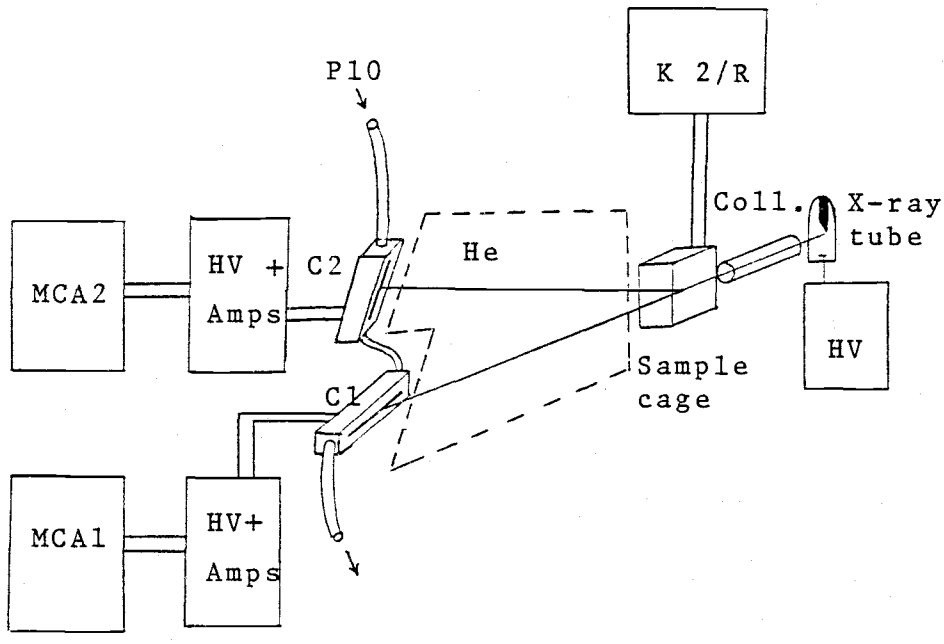

Fig. 10: Set-up for X-ray measurements.

Detector C1 was mounted 210.3 mm away from the sample in a horizontal position. It was placed in the direct beam, which was absorbed by a beam stop. This detector intercepted the low-angle scattering region

up to about 0.18 $Å^{-1}$. Detector C2 was placed 284.8 mm away from the sample, perpendicular to the first one, the normal from the sample to this detector making an angle of about 21° with the direct beam. This detector was responsible for the wide-angle range from 0.16 to 0.37 $Å^{-1}$. The resolution was .093 mm counter wire per channel for detector C1 and .186 mm for detector C2, respectively (corresponding to 1024 and 512 channels for 95 mm effective wire length). With a countrate of around 80 counts per second, some 1,300,000 counts at the low angle detector and approximately 250,000 counts at the wide angle detector were recorded in a typical run.

The temperature was controlled by a Lauda K-2/R temperature regulator, whose accuracy was 0.1°C. Before starting any measurements the sample was incubated at -20°C for at least half an hour and then transferred to the sample cage, which was pre-cooled to the lowest temperature available (about -12°C). If not used for diffraction measurements the sample was kept in a refrigerator at 0.0°C. The temperature range over which measurements were conducted was from -11.5°C up to +40°C. Lower

temperatures cannot be reached by the current apparatus, and higher temperatures are of little interest for this particular sample.

The calibration of the wide angle detector was done with a Calcite powder sample (plus stearic acid crystallites), with peaks at 1/4.12Å and 1/3.68Å for stearic acid, and at 1/3.85Å and 1/3.04Å for calcite (see Fig. 11).

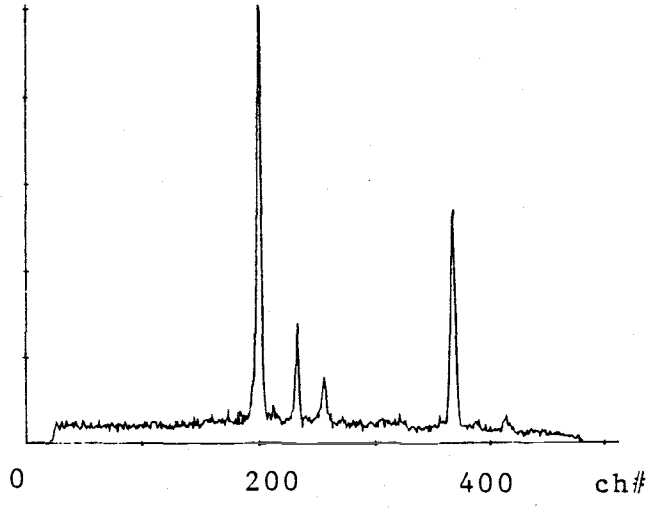

Fig. 11: Wide angle calibration spectrum.

The measured values were evaluated on a computer (program "WIDE.BAS", see Appendix) to determine the angle of the normal to the detector with the direct

beam and the corresponding central channel number.

For the wide angle detector the "central channel" was about 200, the angle of the normal with the direct beam was 21^{o} and the sample-to-detector distance was 284.8 mm, as in previous experiments. The error for getting the correct value for a peak from the channel number in which it is measured was at most 0.6%. For the low angle detector only the central channel number and the sample-to-detector distance were to be determined and found to be 348 and 210.3 mm, respectively. Running these numbers in special programs, the lateral displacement and, hence, the wave vector was determined from the recorded channel numbers.

To check the uniformity of the detector response, runs with the attenuated direct beam only were made for 15 seconds, at 5 mm steps along the detector (see Fig. 12), using a stepping motor. In addition a slow continuous run (in fact 100 fast runs added together) over the entire detector length was also conducted (see Fig. 13). This allowed a correction of the gathered data with respect to any varying sensitivity along the detectors.

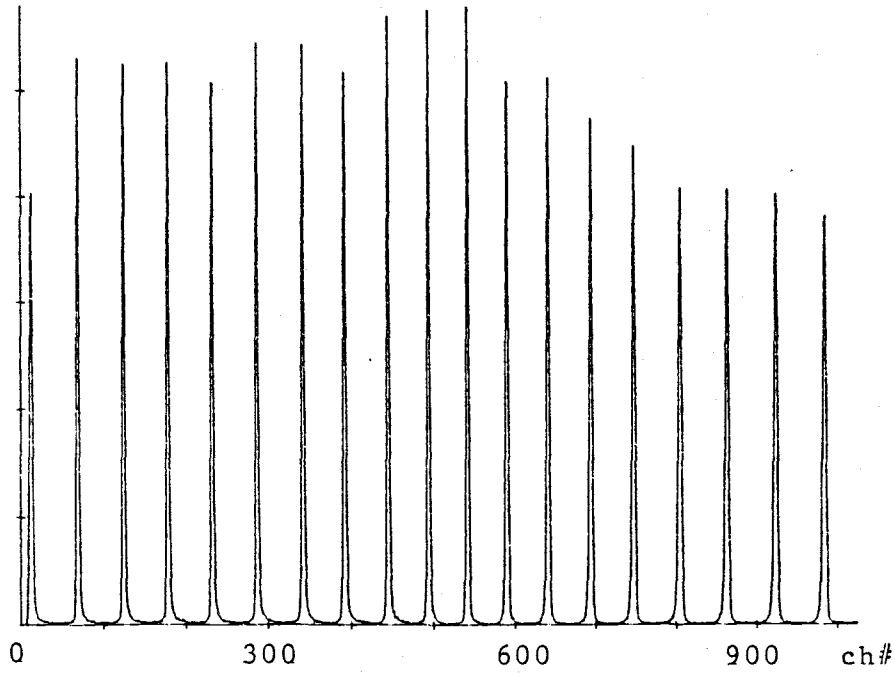

Fig. 12: Counts along the detectors in 5mm steps.

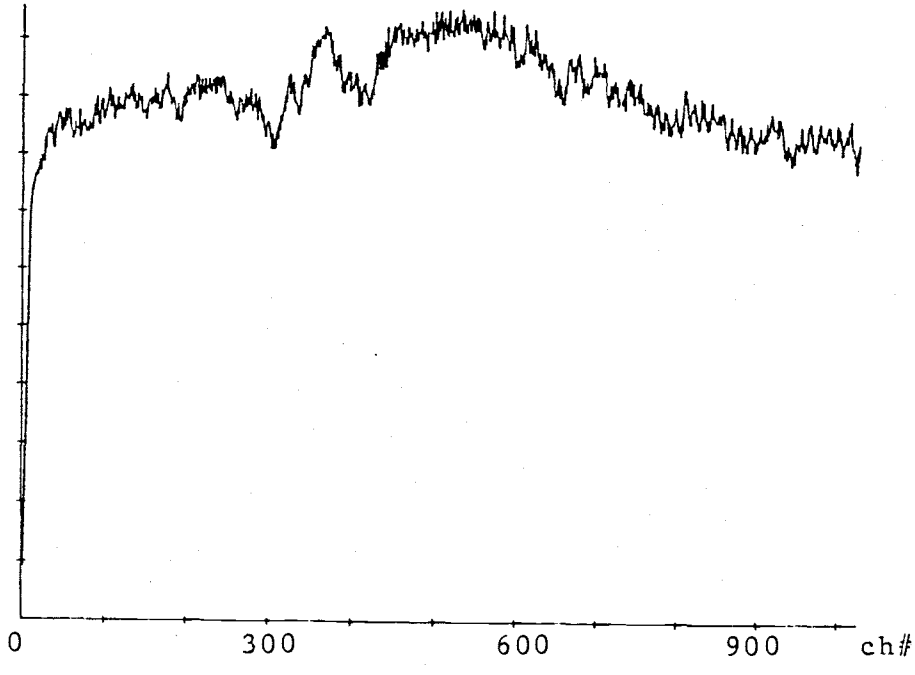

Fig. 13: Continuous detector response.

RESULTS AND DISCUSSION

Phase behavior

Starting at -10°C and gradually heating the sample up, 14 iPC is in the $L_{\beta'}$ or gel phase. This phase is characterized by four clean diffraction orders in the low angle spectrum (see Fig. 14) and some "peaks" - not very sharp - in the wide angle region (see Fig. 15). The sharp peaks in the wide angle region at temperatures below freezing are simply due to scattering from ice around the sample holder. The d-spacing increases continuously with increasing temperature (see Fig. 16), starting from 46 Å at -10°C and ending at 49 Å at -1.0°C, and being most likely due to rearrangement of the headgroups. The side chains in 14 iPC are tilted with respect to the bilayer normal about an angle of approximately 33°, as can be concluded from the different head group-head group separation in the $L_{\beta'}$ and the L_{α} phase.

Upon further heating the sample undergoes a pre-

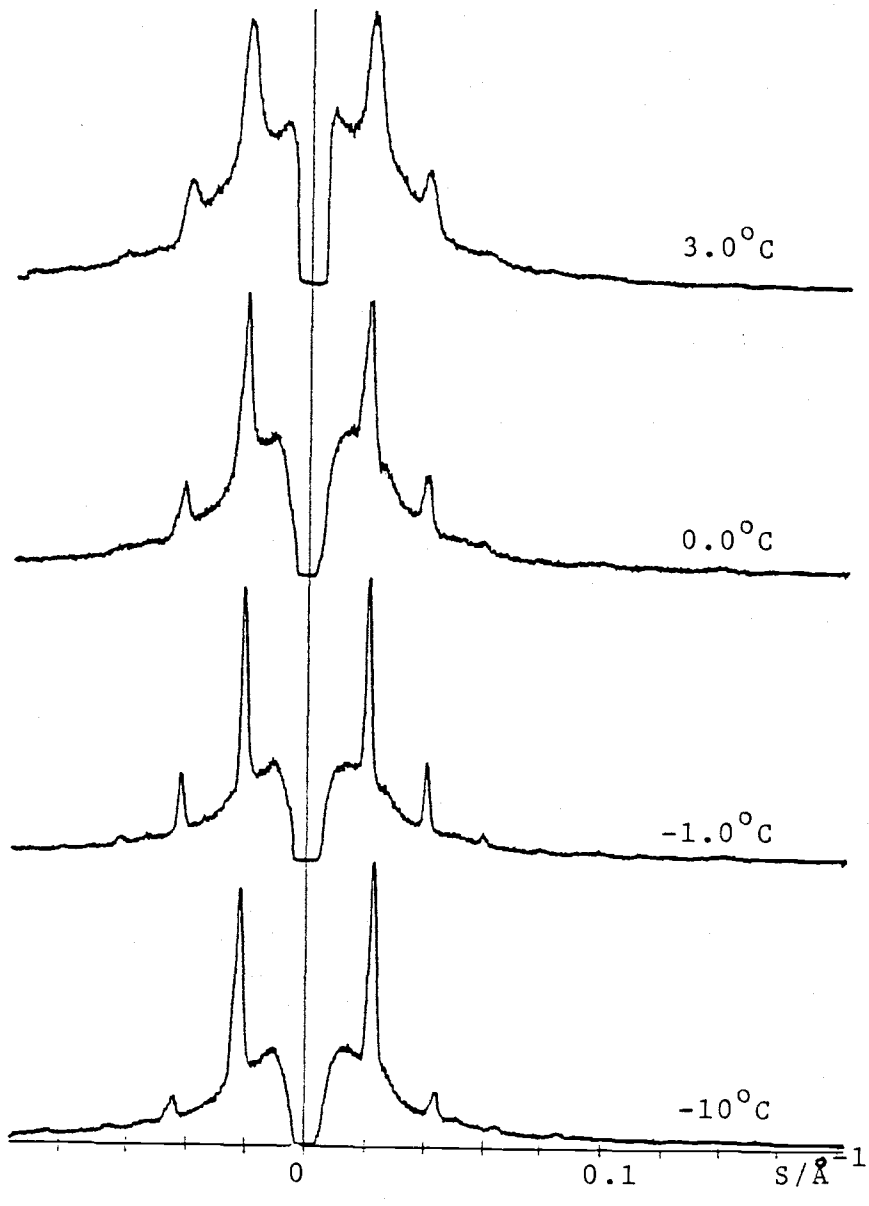

Fig. 14: $L_{\beta'}$ to $P_{\beta'}$ transition of 14 iPC (low angle data).

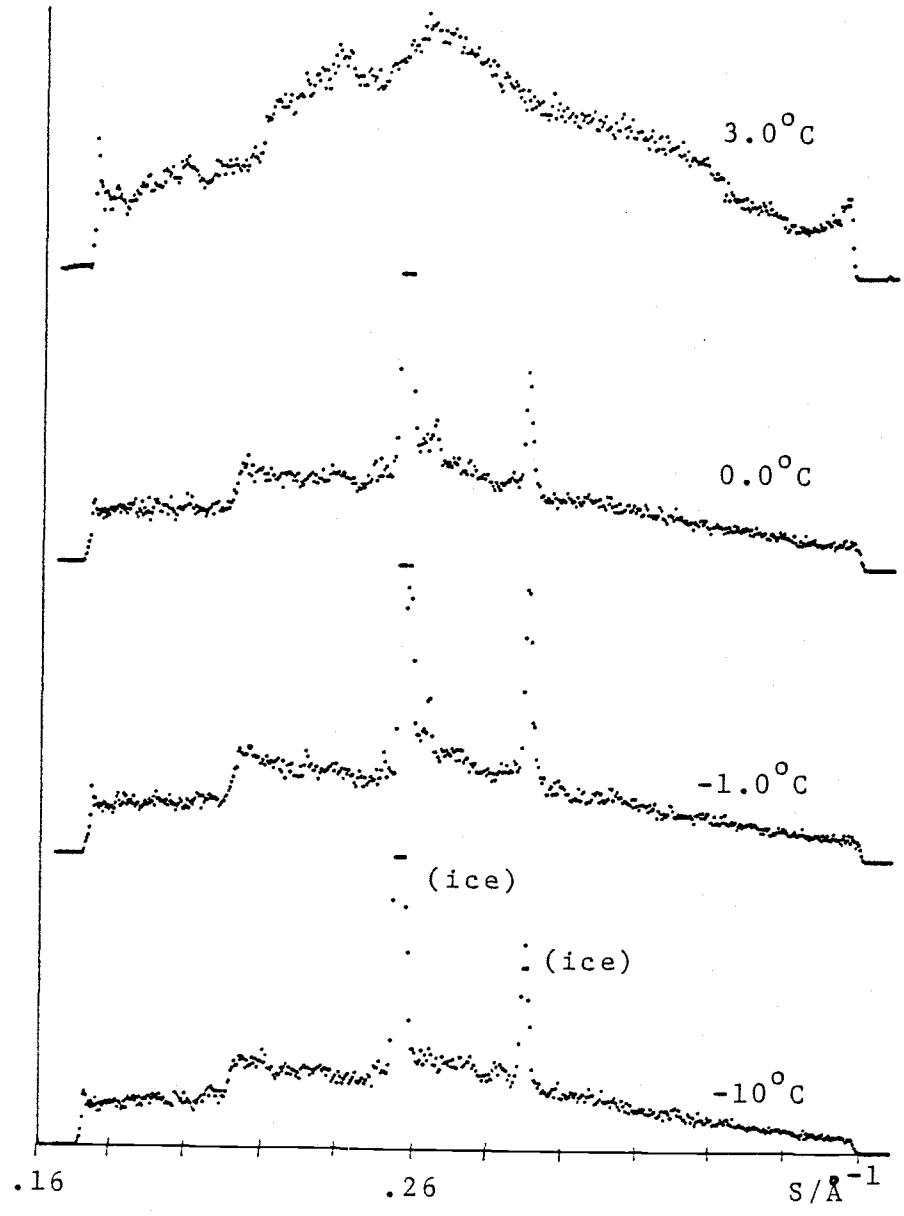

Fig. 15: $L_{\beta'}$ to $P_{\beta'}$ transition of 14 iPC (wide angle data).

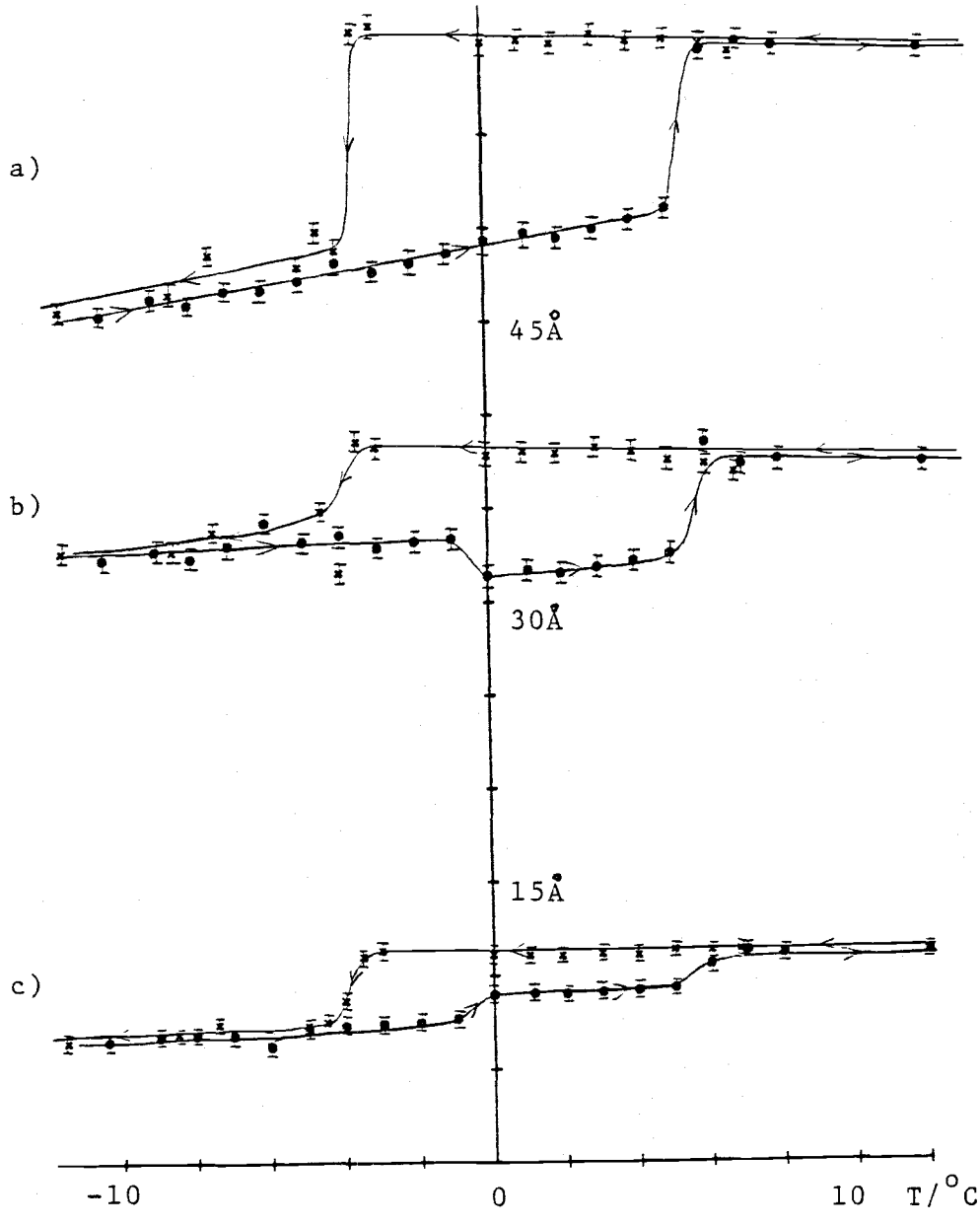

Fig. 16: Characteristic dimensions of 14 iPC bilayers (a = d-spacing, b = head group-head group separation, c = 1/2[a-b]).

transition between -1.0°C and 0.0°C. This is indicated by an increase of linewidth in the small angle spectra, and a decrease of the intensity of the fourth order peak (see Fig. 14). In addition, at temperatures above 0.0°C two broad peaks (at .235 and .265$Å^{-1}$) appear in the wide angle spectrum (see Fig. 15). The new phase is likely to be the $P_{\beta'}$ phase, which is a rippled bilayer gel phase. The characteristic repeat distances associated with the rippling give rise to scattering at small S-values ($\lambda \sim$ 100 - 200 Å). This shows up as an increase in scattered intensity on approach to the beam stop ($S \rightarrow 0$). The higher orders of the very small S scattering show up in broadened lines in the small angle X-ray scattering. Since the d-spacing further on increases linearly (up to 51 Å at 5.0°C), there is also the possibility that the head group-head group separation decreases somewhat at this temperature. The angle of tilt of the side-chains seems to remain about constant.

Between 6.0°C and 6.5°C the main transition to the L_{α} phase (liquid crystal phase) takes place with a co-existence of the $P_{\beta'}$ and L_{α} phases extending over a very narrow temperature interval around 6.0°C of about

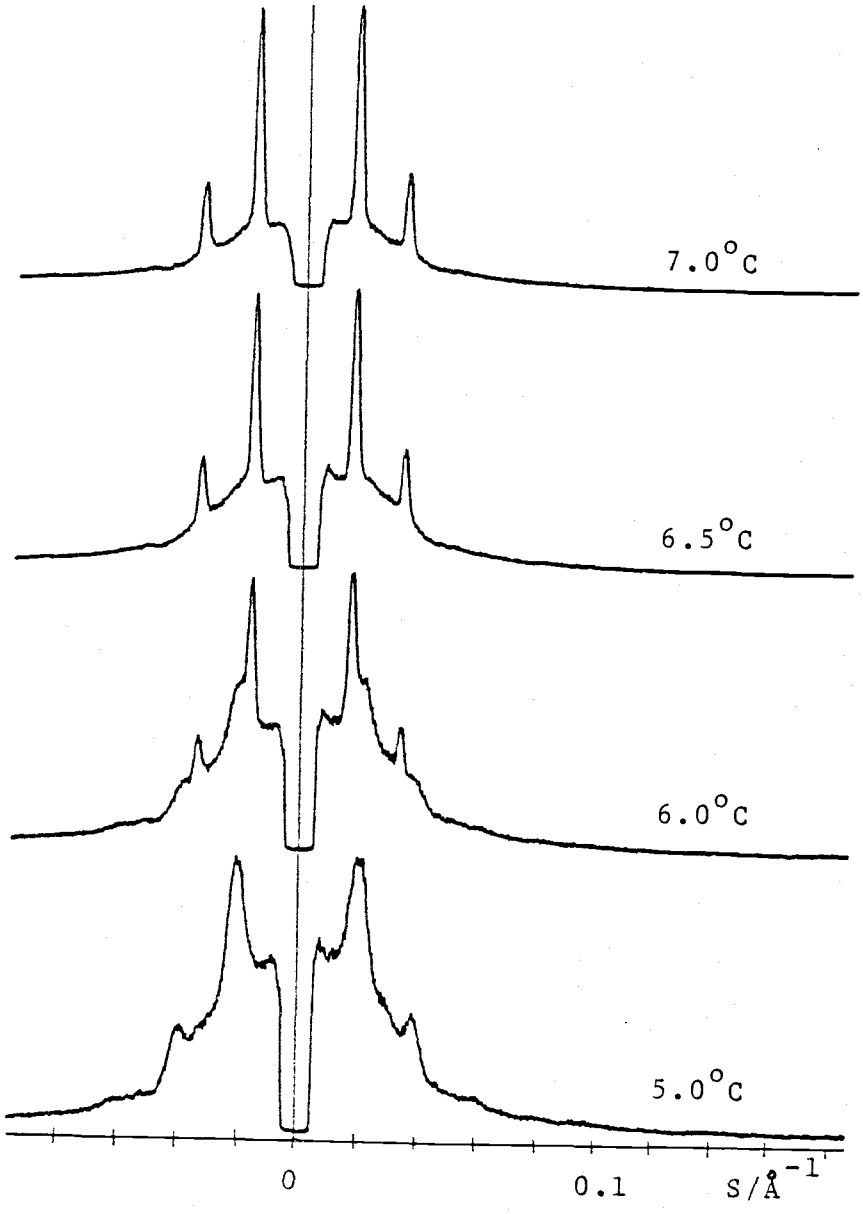

Fig. 17: Gel-liquid crystal transition of 14 iPC (low angle data).

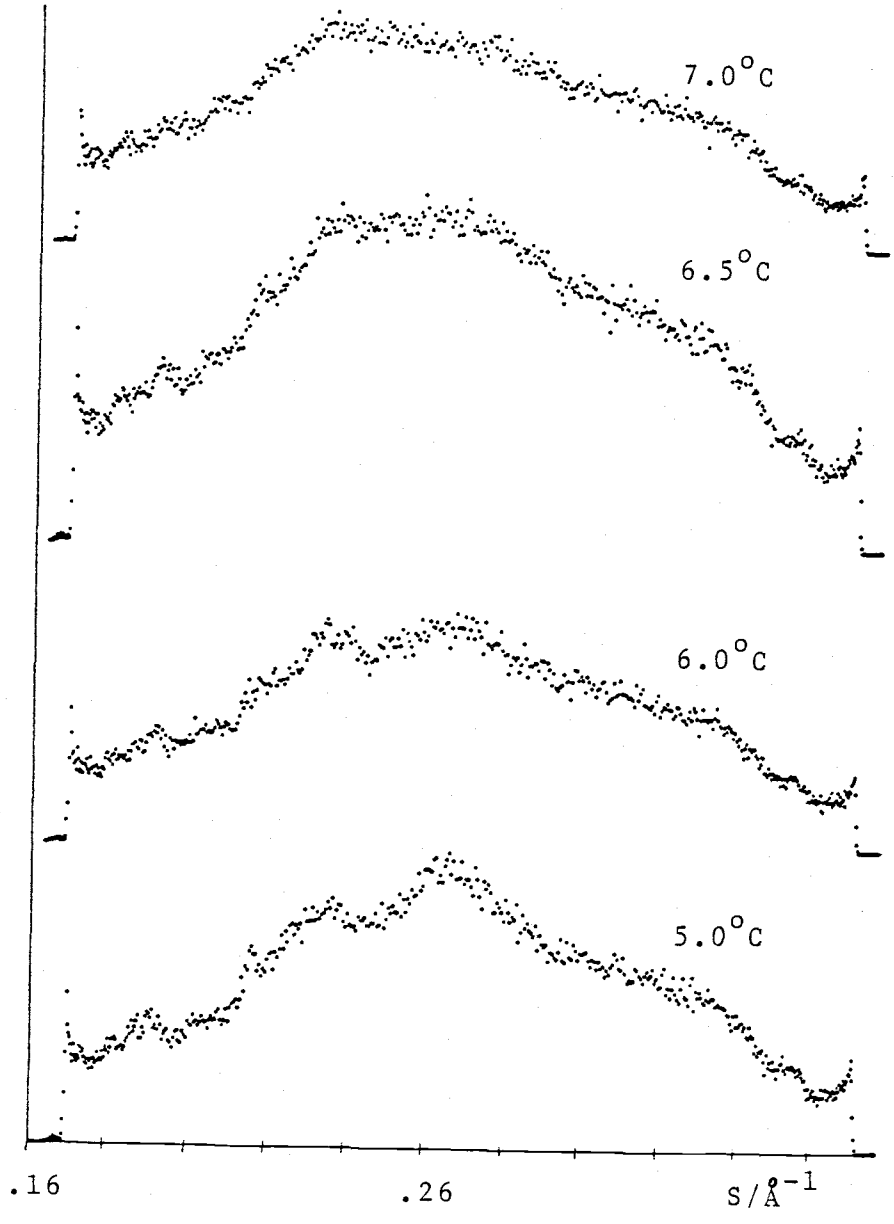

Fig. 18: Gel-liquid crystal transition of 14 iPC (wide angle data).

±0.5°C (see Fig. 17). The low angle diffraction spectrum shows only two sharp lines, characteristic of the liquid crystal phase, while in the wide angle region (see Fig. 18) only a broad hump centered about 1/4 $Å^{-1}$ is present, also characteristic for the L_α phase, indicating melting of the side chains. At this point the d-spacing increases rapidly by 8 Å, of which 6 Å comes from the straightening of the side chains, while the rest is gained by the addition of water between the bilayers.

Additional spectra were taken at temperatures up to 40°C to establish unambiguously the L_α phase, which is thought to be the final high temperature structural form for this kind of system (see Fig. 19).

Gradually cooling down the sample from 12°C showed a persistence of the L_α phase alone down to between 5.0°C and 4.0°C, where the $P_{\beta'}$ phase appeared again, but with the L_α phase still dominating. We find co-existence of both phases down to 0.0°C, where the $P_{\beta'}$ disappears almost completely, most likely converted back to L_α over time (see Figs. 20,21).

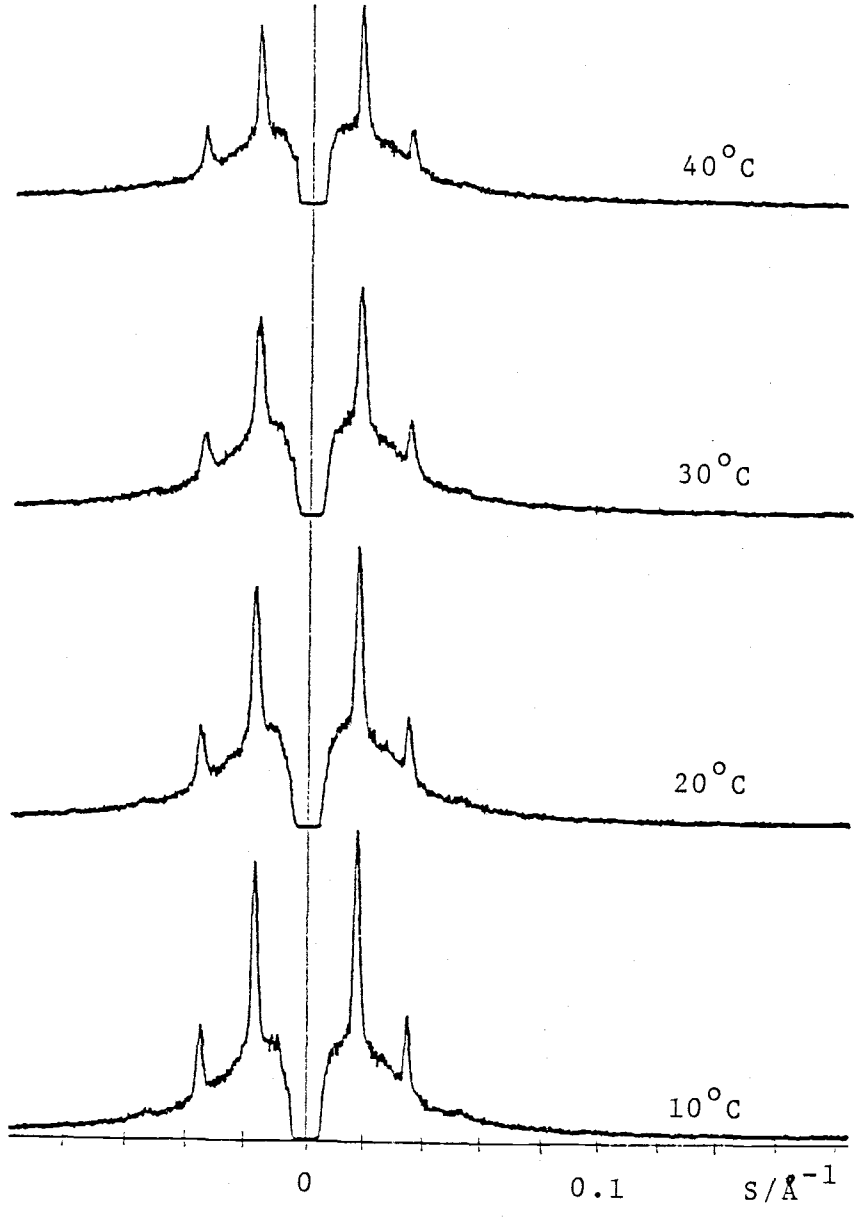

Fig. 19: high temperature behavior of 14 iPC.

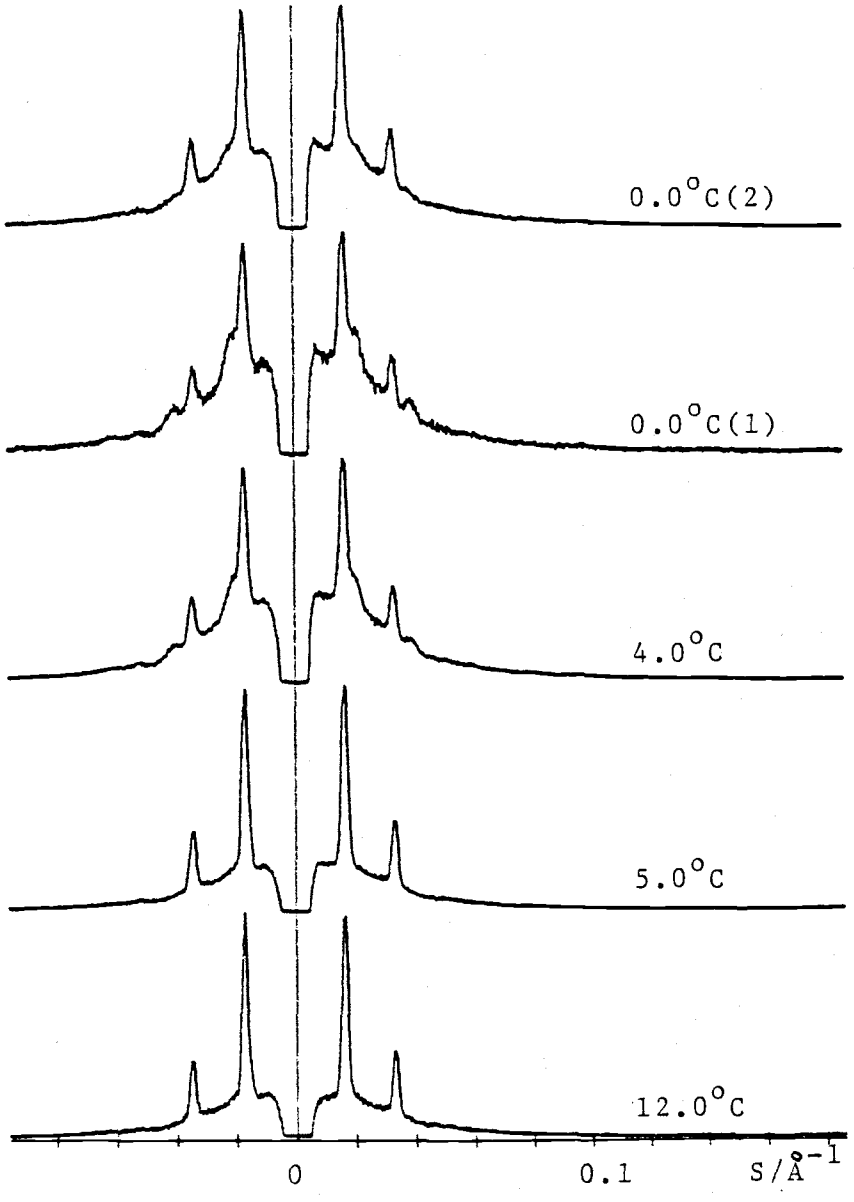

Fig. 20: Cooling below gel-liquid crystal transition (low angle data).

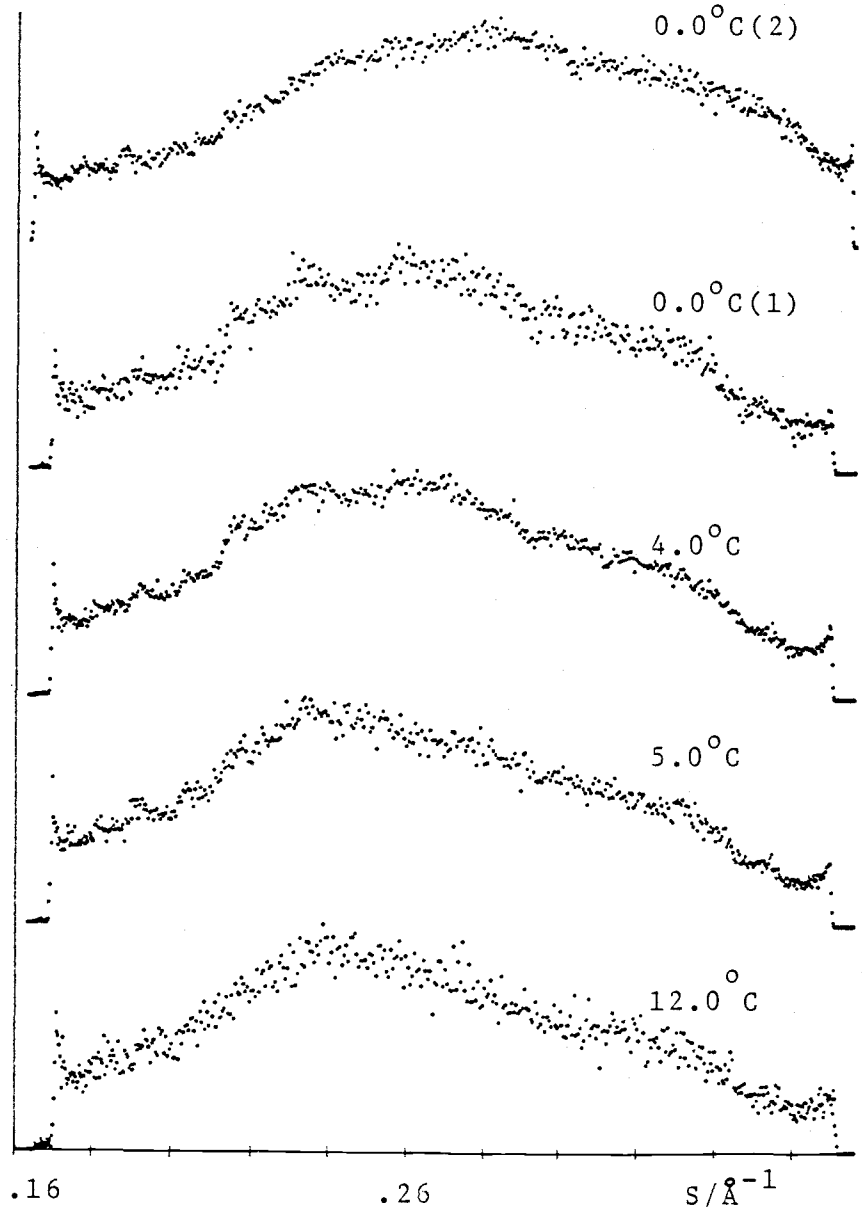

Fig. 21: Cooling below gel-liquid crystal transition (wide angle data).

Rapid cool-down from 12°C to 1.6°C brought up both L_{α} and $P_{\beta'}$ phases, yet sitting at this temperature for 90 hrs did not reveal any relaxation effects (see Figs. 22,23). Another rapid cool-down to -3.0°C showed that the L_{α} phase can persist as the unique phase present down to -3.0°C (see Fig. 24). Only between about -3.5°C and -4.0°C does one find co-existence of the L_{α} and the $P_{\beta'}$ phases. $P_{\beta'}$ has established itself as the unique phase at -4.5°C and persists down to -9.0°C. Between -9.0°C and -10°C the back-transition into the $L_{\beta'}$ phase takes place. The low angle spectrum shows for the $P_{\beta'}$ phase a low diffraction intensity in this temperature region, while the wide angle spectrum (see Fig. 25) exhibits the same pattern as for the heating mode.

Cycling from -10°C to 0.0°C and back down again produced the same small angle diffraction spectra, at the same temperatures, thus showing reversibility in the $L_{\beta'}$ phase.

During a run at -12°C, it was found that although the low angle diffraction does not differ from the one at -11°C, the wide angle spectrum shows definitely

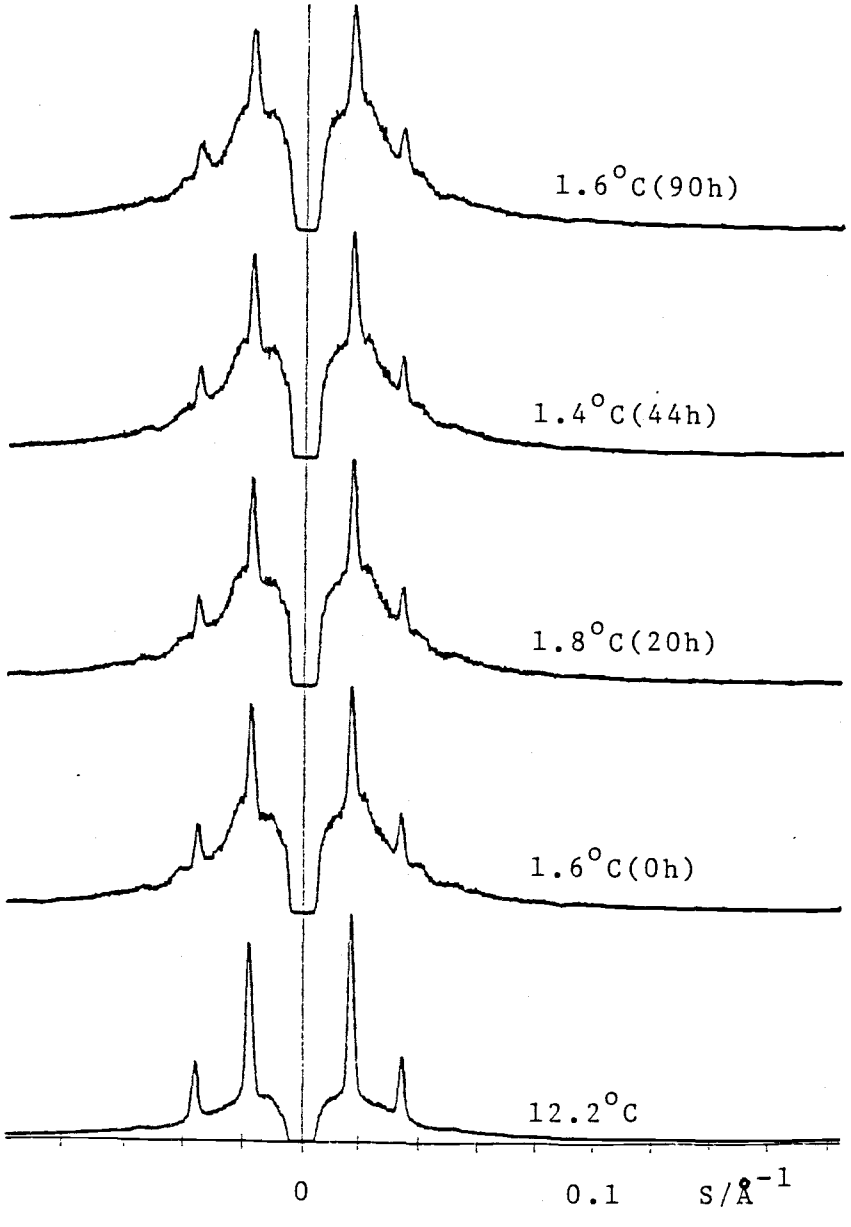

Fig. 22: Stability of intermediate phase (low angle data).

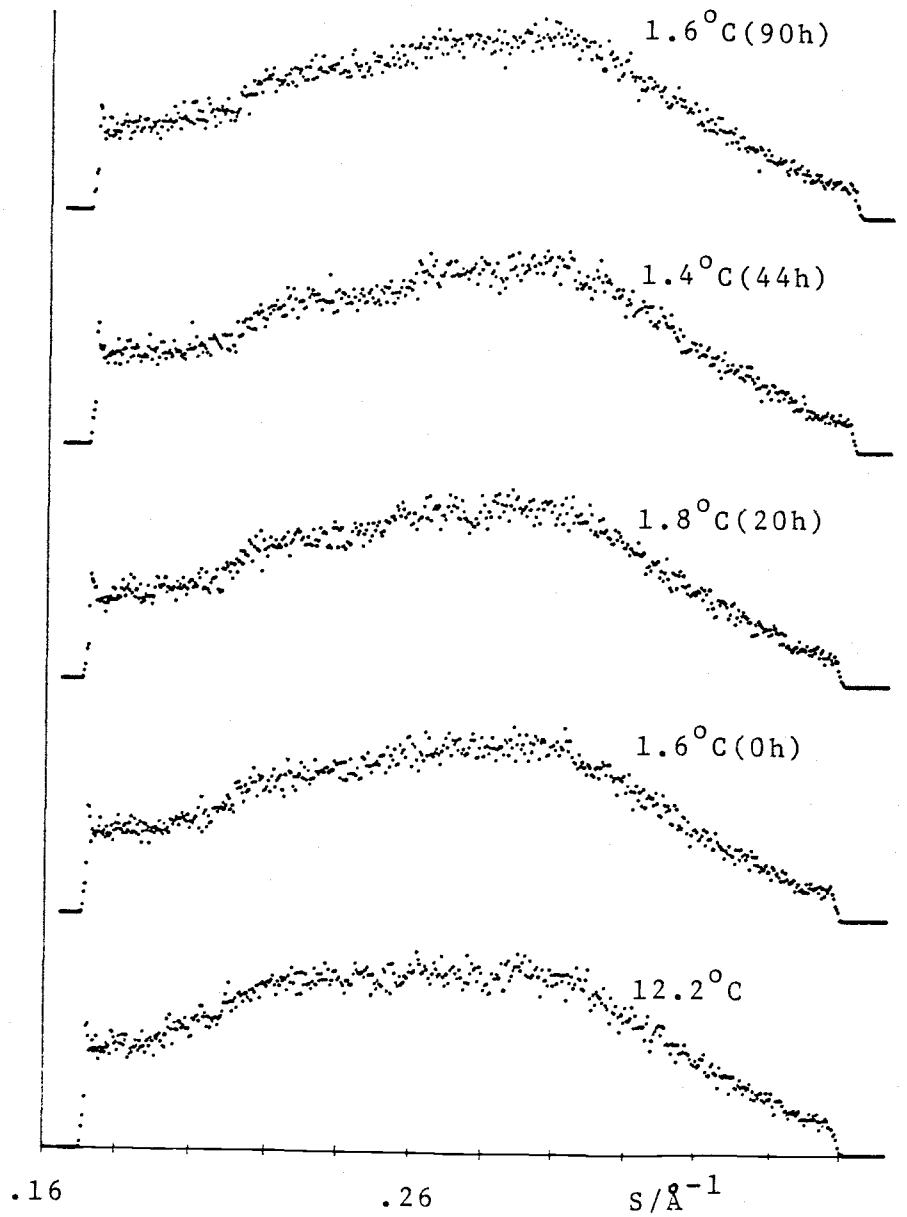

Fig. 23: Stability of intermediate phase (wide angle data).

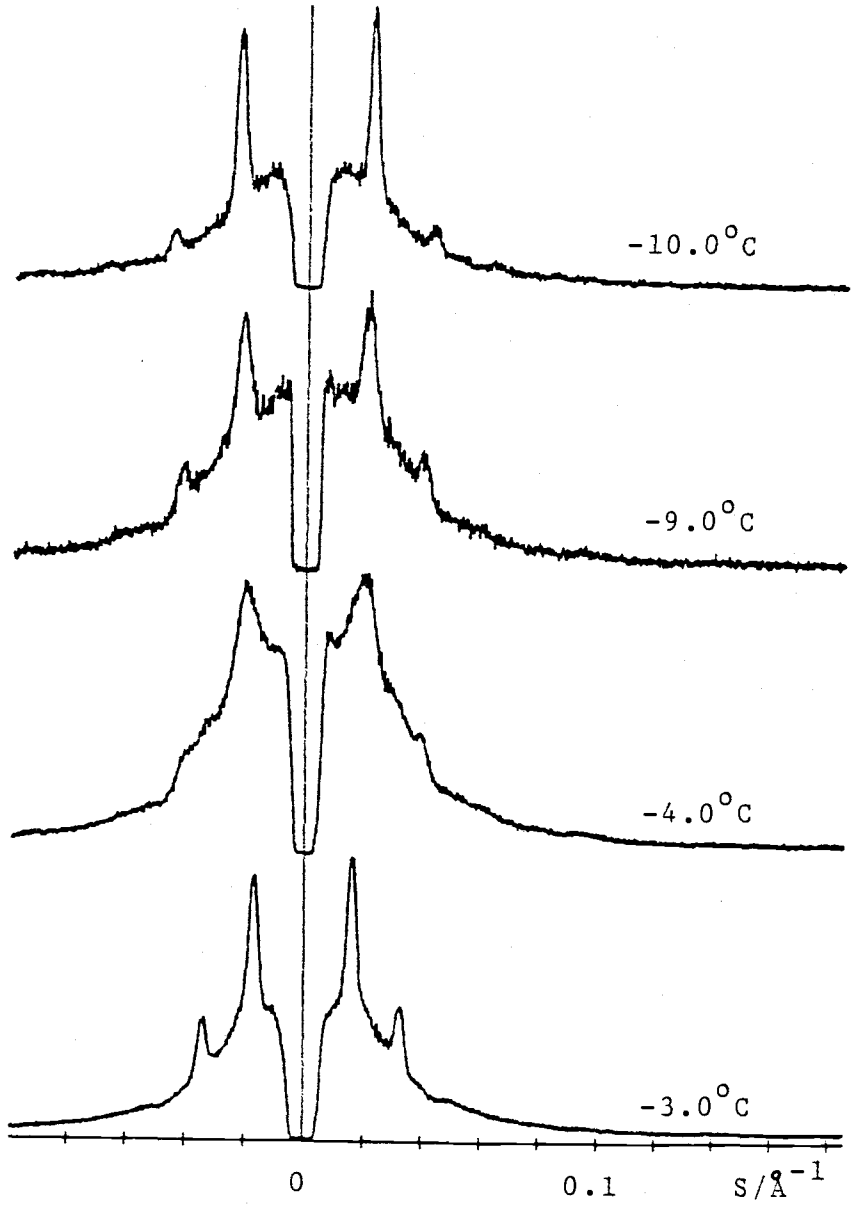

Fig. 24: Back-transition into $L_{\beta'}$ phase (low angle data).

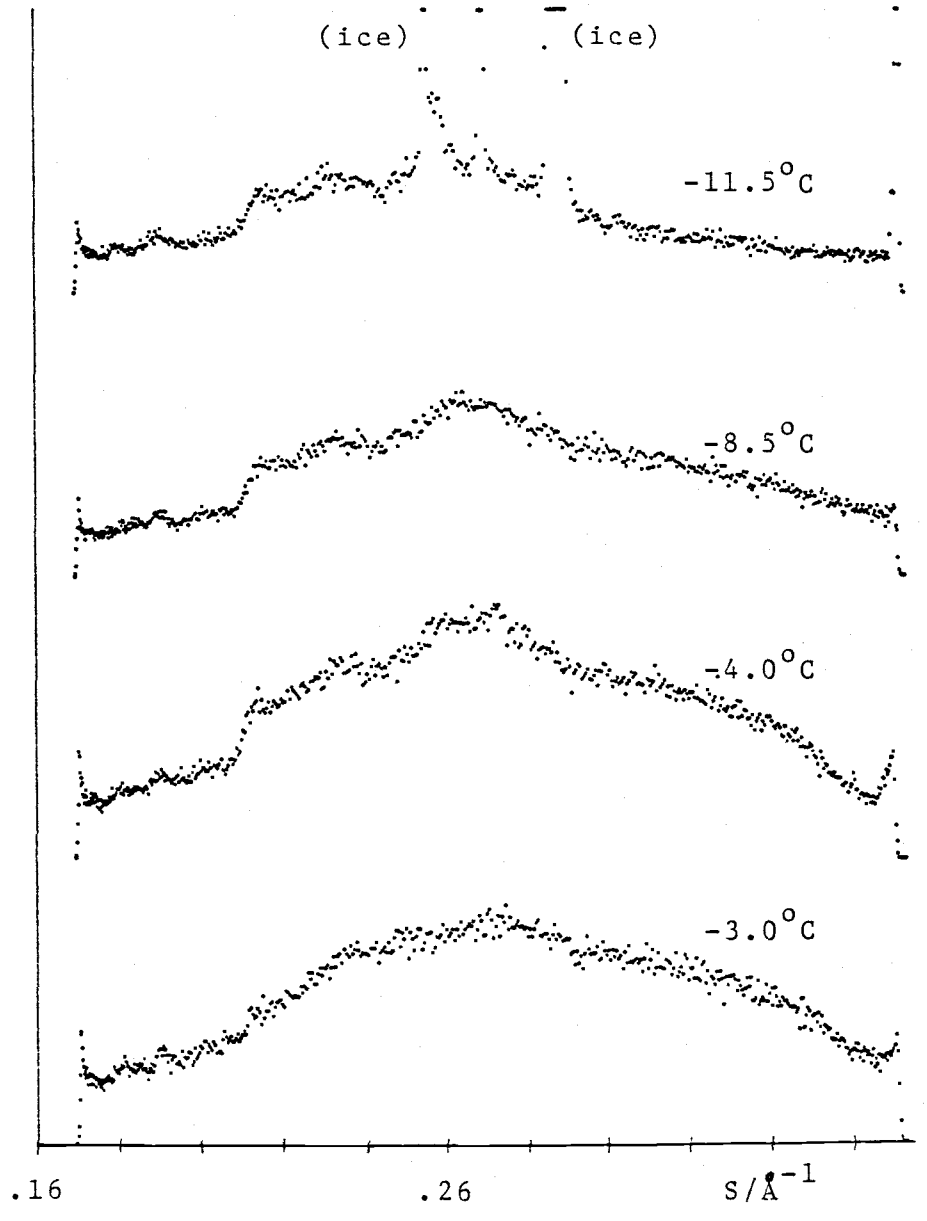

Fig. 25: Back-transition into $L_{\beta'}$ phase (wide angle data).

structured, sharp peaks (see Fig. 26). This may indicate that 14 iPC enters a subgel phase at temperatures of -12°C and below. Unfortunately, with the current apparatus this temperature region cannot be explored.

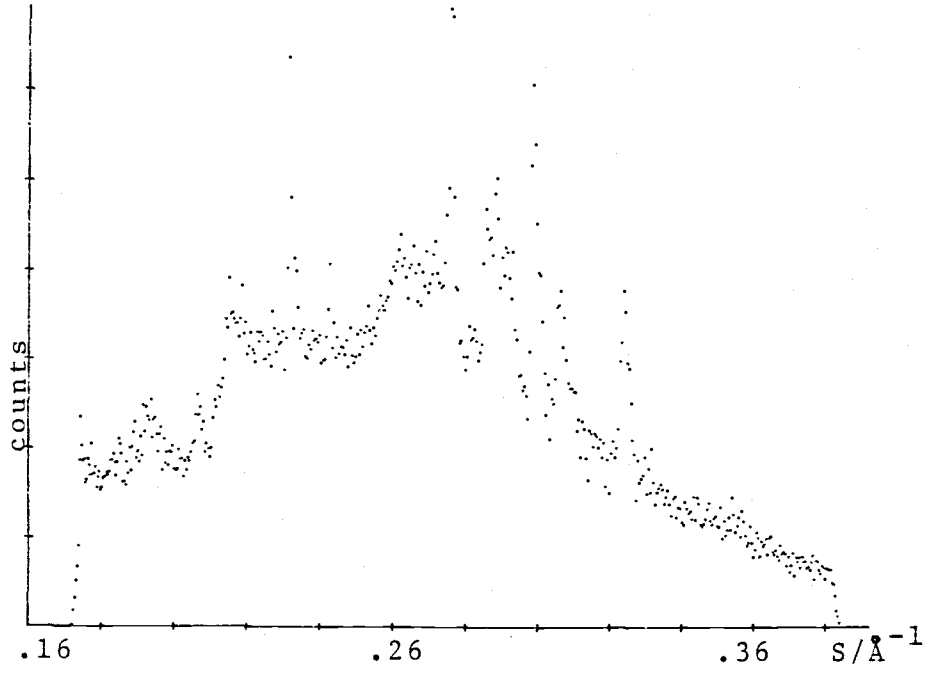

Fig. 26: Structured wide angle spectrum (-12°C).

Electron density models

Using the model for disordered multibilayers discussed by Blaurock (1982), one can try to fit certain electron density profiles to the data gathered. Knowing the general structure of the bilayer, we expect a rather high electron charge density around the phosphorus atom in the headgroup, and a relatively low electron charge density around the terminating methyl groups in the bilayer center. Therefore, a distribution like Fig. 27 seems reasonable. This profile was constructed using a pair of Gaussians.

Since the Fourier transform of a Gaussian is again a Gaussian, the diffraction pattern can be obtained easily (see Fig. 28).

Multiplying this intensity-profile with the appropriate interference function (here, the number of bilayers is taken to be 10 and the pair-correlation function h(x), which is also a Gaussian, is assigned a width of 6 Å, which means the repeat distances fall in general into an interval of ±3 Å around the mean value)

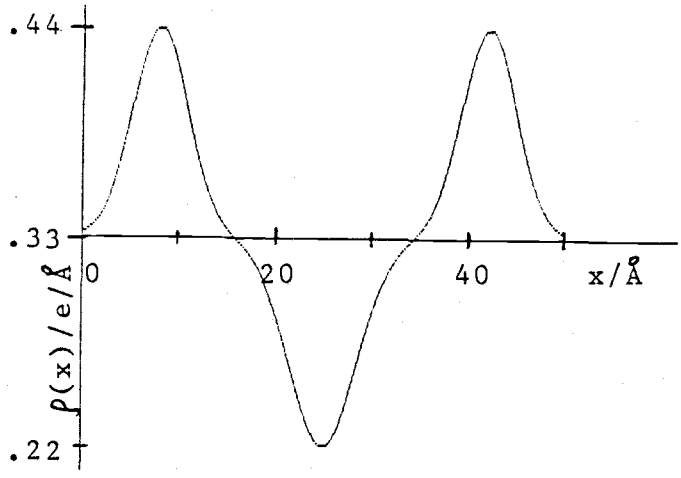

Fig. 27: Model electron density distribution of one bilayer.

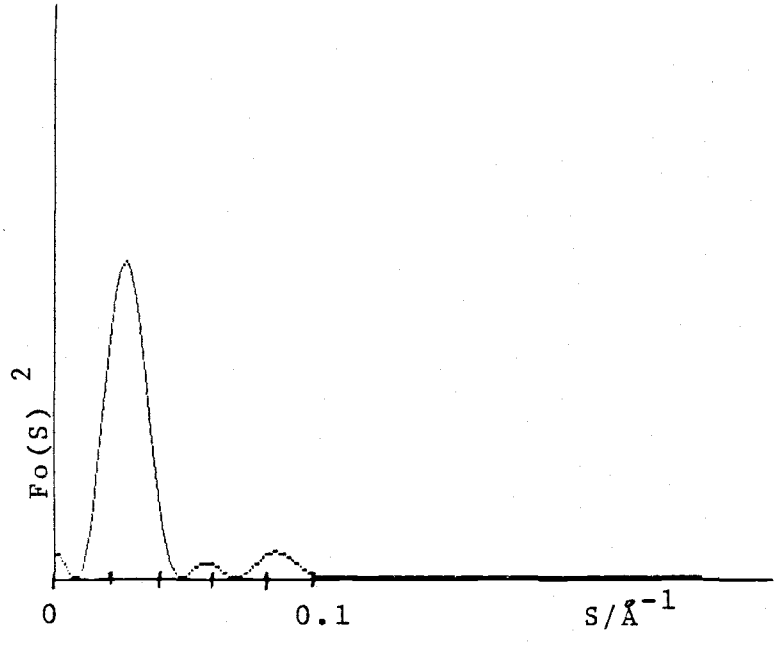

Fig. 28: Diffraction pattern of the bilayer.

yields then the intensity of the various diffraction orders, that can be expected (see Fig. 29).

Comparing these results to the gathered data sufficient agreement is found to justify the assumption made for the electron density. To fit the model to the different phases, adjustments of the positions of the "peaks" for the head group density as well as the width of all "peaks" is neccessary.

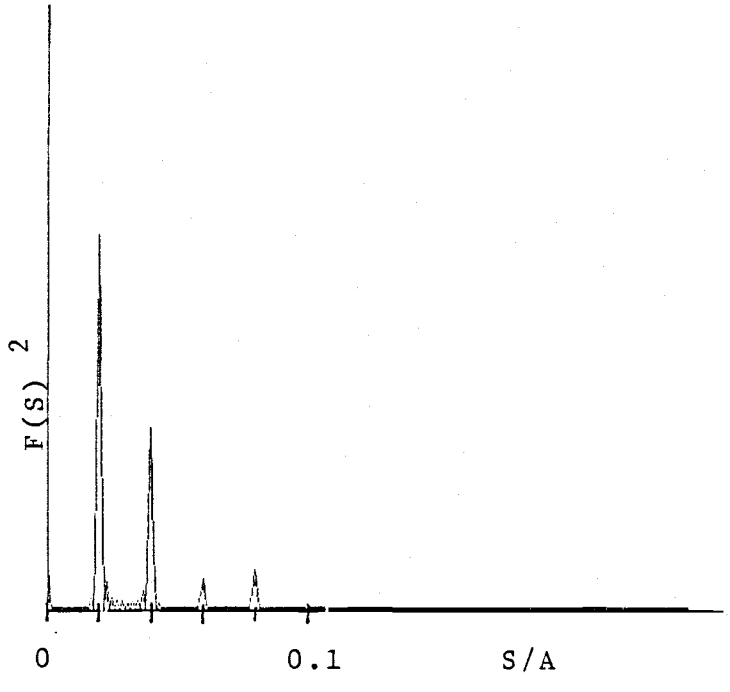

Fig. 29: Diffraction pattern of 10 disordered bilayers.

Another approach is to calculate the ratios of the scattering amplitudes from the X-ray diffraction spectra, and to choose the phase factors. Using these data, the corresponding electron density can be calculated. The results obtained by this method match the electron density distributions assumed above for our model. Thus it can be stated with some confidence that the assumed model characterizes the electron charge density along the bilayer normal fairly well, and also that the choice for the phase factors (-1, -1, +1, -1, respectively, for the first four orders) is likely to be correct. In addition, an increase in the linewidth with increasing scattering angle indicates, that disorder of the second kind is present in these types of bilayers.

Comparison to DSC results

Using Differential Scanning Calorimetry, Lewis and McElhaney (1985) found two transition temperatures for 14 iPC. By heating up the sample, they discovered an endotherm at 7.6^{o}C, while by cooling down they found

an exotherm at -5.2°C. In their work they labeled these temperatures T_m and T_f, respectively. Also, they found that the transition at 7.6°C only took place if the sample was previously cooled down below -5.2°C, while the transition at -5.2°C only was picked up if the sample was first heated above 7.6°C. Although these temperatures do not quite agree with the ones found in our X-ray measurements (because of the fast heating and cooling rates in DSC measurements, sometimes the sample undergoes a transition when the corresponding temperature was already passed), an analogous behavior of 14 iPC could be determined. It seems, that the phase transitions are triggered by different events in the heating and cooling mode. DSC studies of several n-iPCs showed that the endotherm of the smaller chain iPCs are subject to hysteresis. This can be confirmed for 14 iPC from the gathered X-ray data, as shown directly by the supercooling of the L_α phase.

CONCLUSION

Bilayers constructed from 14 iPC reveal a phase behavior somewhat different from those previously studied and based on 16 nPC (DPPC) and 17 iPC. At room temperature it is always in the liquid crystal (L_α) phase, with a d-spacing of 59 to 60 Å. Starting at -10°C, it is in the $L_{\beta'}$ phase, characterized by four clean peaks in the low angle region. Between -1.0°C and 0.0°C it transforms into the rippled gel phase ($P_{\beta'}$), with mainly two broad orders in the low angle region and two broad peaks in the wide angle region. Above 6.5°C, it finally resumes the L_α phase, characterized by only two sharp low angle peaks and a broad hump in the wide angle region, indicating fluidization of the side chains. Like DPPC (but unlike 17 iPC) the side chains are canted about the bilayer normal, about an angle of 33°. Although the side chains are only two methylene groups shorter (about 2 Å) than those of 16 nPC, the d-spacing in the gel phase is much smaller than for DPPC (46 to 49 Å compared to 63 Å for DPPC), and also smaller than for 17 iPC (61 Å). The transition temperatures are much lower than those found for DPPC (see Fig. 30).

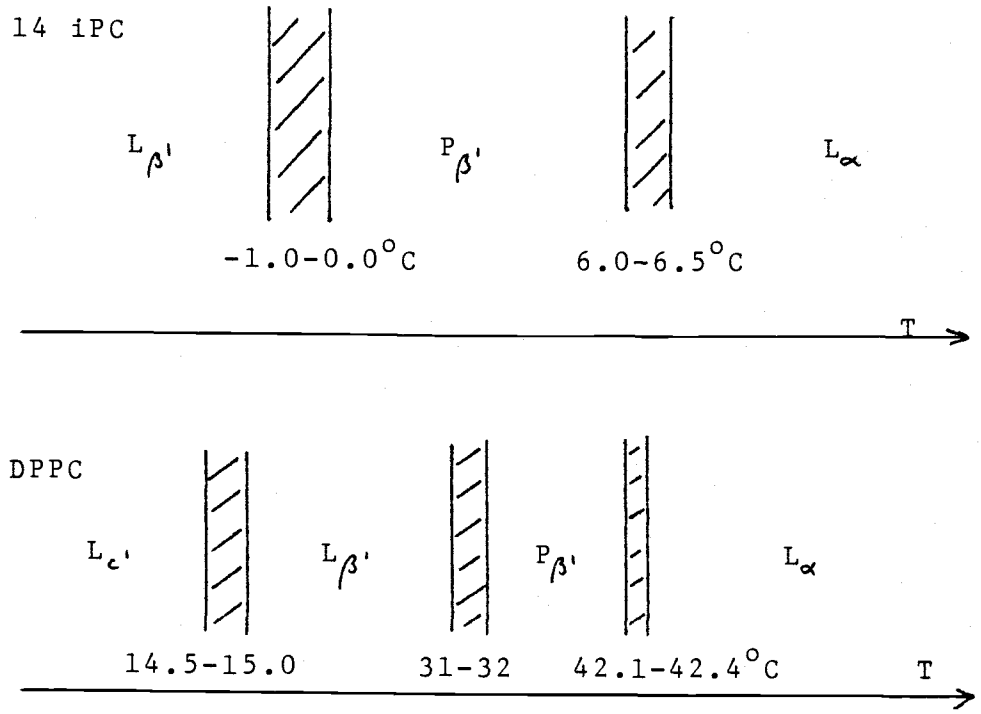

Fig. 30: Transition temperatures for 14 iPC and DPPC.

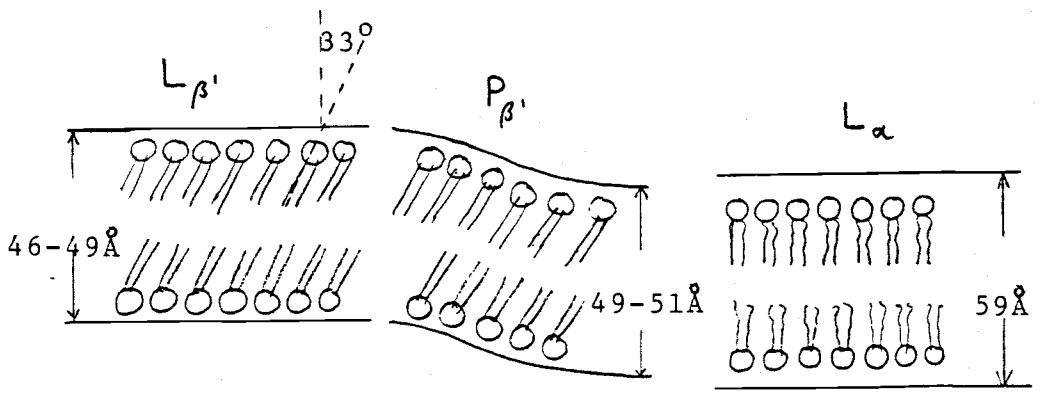

Fig. 31: Lamellar structures of 14 iPC.

Fig. 31 illustrates the lamellar structures of 14 iPC. These are similar to those for DPPC, but different from 17 iPC, which has only straight chains, and 20 iPC, which has canted chains in the subgel phase only. The thermotropic phase behavior of 14 iPC is not fully reversible, as can be demonstrated by supercooling the L_{α} phase. Therefore, whenever data about 14 iPC are published, knowing the history of the sample is essential.

BIBLIOGRAPHY

Ansel,G.B.;Hawthorne,J.N.: Phospholipids,
Elsevier Publishing Co. (1964)

Bell,R.J.: Introductory Fourier Transform spectroscopy,
Academic Press (1972)

Blaurock,A.E.: Evidence of bilayer structure and of membrane interactions from X-ray diffraction analysis,
Biochimica et Biophysica Acta(1982), 650, 167

Blaurock,A.E.;Nelander,J.C.: Disorder in nerve myelin: Analysis of the diffuse X-ray scattering,
J.Mol.Biol. (1976), 103, 421

Champeney,D.C.: Fourier Transforms and their physical applications,
Academic Press (1973)

Chapman,D.: The structure of lipids by spectroscopic and X-ray techniques,
John Wiley & Sons (1965)

Church,S.E.; Griffiths,D.J.; Lewis,R.N.A.H.; McElhaney, R.N.; Wickman,H.H.: X-ray structure study of thermotropic phases in isoacylphosphatidylcholine bilayers,
Biophysical Journal (1986), 49, 597

Davenport,J.B.; Johnson,A.R.: Biochemistry and methodology of lipids,
Wiley Interscience (1971)

DeVries,J.L.; Jenkins,R.: Worked examples in X-ray analysis,
Macmillan (1971)

Franks,N.P.;Liab,W.R.: The structure of lipid bilayers and the effects of general anaesthetics,
J.Mol.Biol. (1979), 133, 469

Gbordzoe,M.K.;Kreutz,W.: Direct X-ray determination of the electron density profile of the nerve myelin membrane, with paracrystalline lattice distortions taken into account,
J.Appl.Cryst. (1978), 11, 489

Gbordzoe,M.K.;Kreutz,W.: Comments on the para-crystalline nature of myelin, J.Appl.Cryst. (1978), 11, 701

Goodman,J.W.: Introduction to Fourier-optics, McGraw-Hill Book Co (1968)

Gray,G.W.;Goodby,J.W.G.: Smectic liquid crystals, Leonard Hill (1984)

Hentschel,M.; Hosemann,R.: Small and wide angle X-ray scattering of oriented lecithin multilayers, Mol.Cryst.Liq.Cryst.(1983), 94, 291

Hosemann,R.;Bagchi,S.N.: Direct analysis of diffraction by matter, North Holland Publishing Co (1962)

Hukins,D.: X-ray Diffraction by disordered and ordered systems, Pergamon Press (1981)

Lehninger,A.L.: Biochemistry, Worth Publishing Inc. (1975), 2nd edition

Levine,Y.K.: X-ray diffraction studies of membranes, Progr.Surf.Membr.Sci. (1973), 3, 279

Lewis,R.N.A.H.; McElhaney,R.N.: Thermotropic phase behavior of model membranes composed of phosphatidylcholines containing iso-branched fatty acids: I. Differential scanning calorimetric studies, Biochemistry (1985), 24, 2431

Lipson,H.; Taylor,C.A.: Fourier transforms and X-ray diffraction, G. Bell & Sons (1958)

Lipson,H.; Taylor,C.A.: Optical Transforms, Cornell University Press (1965)

Lytz,R.K.: Ph.D. Dissertation, OSU (1978)

Matsuo,M.: One dimensional mathematical treatment of small angle X-ray scattering from a system of alternating lammellar phases, J.Chem.Soc. FT II (1983), 79, 1593

McElhaney,R.N.; Silvius,J.R.: Effects of Phospholipid acyl chain structure on physical properties: I. Isobranched phosphatidylcholines, Chem.Phys.Lipids (1979), 24, 287

Pape,E.H.: X-ray small angle scattering, Biophysical Journal (1974), 14, 284

Schwartz,S.;Cain,J.E.;Dratz,E.A.;Blasie,J.K.: An analysis of lamellar X-ray diffraction from disordered membrane multilayers with application to data from retinal rod outer segments, Biophysical Journal (1975), 15, 1201

Torbet,J.;Wilkins,M.H.F.: X-ray diffraction studies of lecithin bilayers, J.Theor.Biol. (1976), 62, 447

Vainshtein,B.: Diffraction of X-rays by chain molecules, Elsevier Publishing Co (1966)

Wilson,A.: Elements of X-ray Crystallography, Addison Wesley (1970)

Worthington,C.R.;King,G.I.;McIntosh,T.J.: Direct structure determination of multilayered membrane-type systems which contain fluid layers, Biophysical Journal (1973), 13, 480

Zaccai,G.;Blasie,J.K.;Schoenborn,B.P.: Neutron diffraction studies on the location of water in lecithin bilayer model membranes, Proc.Nat.Acad.Sci.USA (1975), 72, 376

A P P E N D I X

Program "Wide" (BASIC) to determine the wide angle counter parameters:

```
10 REM      WIDE.BAS
20 REM      PROGRAM TO DETERMINE WIDE ANGLE COUNTER PARAMETERS
30 REM
31 REM      YOU INPUT XSD (SAMPLE-TO-DETECTOR-DISTANCE)
32 REM      AND THE CALIBRATION PARAMETERS X0,X1,X2,X3
40 REM
50 REM      TRY VARIOUS VALUES OF THETA (THE ANGLE THE
51 REM      PERPENDICULAR OF THE COUNTER MAKES WITH THE BEAM)
52 REM
60 REM      ALSO YOU HAVE TO TRY VARIOUS VALUES FOR
61 REM      THE CENTRAL CHANNEL
70 REM
71 REM
72 REM      THIS PROGRAM USES THE COEFFICIENTS X0,X1,X2,X3
73 REM      FOR THE CALIBRATION #10 ONLY!
74 REM
75 REM
80 X0 = -2.48508
90 X1 = .123267
100 X2 = 3.50268E-04
110 X3 = -3.77007E-07
120 XSD = 284.8
121 PRINT
130 INPUT "ANGLE PERPENDICULAR LINE MAKES WITH BEAM : ";THETA
140 INPUT "CHANNEL NO AT PERPENDICULAR POSITION : ";NC
150 THETA = THETA*3.14159/180
160 TANG = TAN(THETA)
170 RD = X0+X1*NC+X2*NC*NC+X3*(NC^3)
180 N = 368    :REM     CALCITE CHANNEL NO
190 GOSUB 500
191 PRINT
200 PRINT "1/Q CALCITE (3.04 A)",1/Q
210 PRINT "RELATIVE % ERROR",(1/Q-3.04)*100/3.04
220 N = 256    :REM     CHANNEL NO FOR STEARIC ACID (3.68 A)
230 GOSUB 500
231 PRINT
240 PRINT "1/Q STEARIC ACID (3.68 A)",1/Q
250 PRINT "RELATIVE % ERROR",(1/Q-3.68)*100/3.68
260 N = 233    :REM      CHANNEL NO FOR STEARIC ACID (3.85 A)
270 GOSUB 500
271 PRINT
280 PRINT "1/Q STEARIC ACID (3.85 A)",1/Q
290 PRINT "RELATIVE % ERROR",(1/Q-3.85)*100/3.85
300 N = 200     :REM     CHANNEL NO FOR STEARIC ACID (4.12 A)
310 GOSUB 500
311 PRINT
320 PRINT "1/Q STEARIC ACID (4.12 A)",1/Q
330 PRINT "RELATIVE % ERROR",(1/Q-4.12)*100/4.12
340 N = 1       :REM     LOWEST CHANNEL NO
350 GOSUB 500
351 PRINT
360 PRINT "1/Q CALCULATED FOR CHANNEL 1",1/Q
370 N = 512    :REM    HIGHEST CHANNEL NO
380 GOSUB 500
390 PRINT "1/Q CALCULATED FOR CHANNEL 512",1/Q
400 THETA = THETA*180/3.14159
401 PRINT
410 PRINT "ANGLE TO BEAM ",THETA
411 PRINT "PERPENDICULAR CHANNEL ",NC
420 PRINT
```

Program "Wide" (continued):

```
421 PRINT
422 PRINT " TO CHECK DPPC TYPE '1' "
423 PRINT " TO TRY ANY OTHER COMBINATION OF THETA AND NC TYPE '0'"
424 PRINT " HIT ANY OTHER NUMBER TO EXIT THE PROGRAM "
430 INPUT U
440 IF U=1 GOTO 445 ELSE GOTO 441
441 IF U=0 GOTO 10 ELSE END
445 REM
446 REM     TEST FOR DPPC-PEAK AT 4.20 A
447 REM
448 PRINT
449 REM
450 INPUT "INPUT THE CHANNEL NUMBER ";N
460 GOSUB 500
465 PRINT
470 PRINT "1/Q FOR CHOSEN CHANNEL",1/Q
471 PRINT "RELATIVE % ERROR FOR DPPC (4.20 A)",(1/Q-4.2)*100/4.2
480 GOTO 420
500 X=X0+X1*N+X2*N*N+X3*(N^3)
510 T = (X-RD+XSD*TANG)/(XSD-(X-RD)*TANG)
520 Q = 1.2972*SIN(.5*ATN(T))
530 RETURN
```

Program "Electron density" (TURBO-PASCAL) to plot model electron densities, using Gaussian functions:

```
program electron_density (input,output);
{  program to plot model electron densities  }
var a,alpha,b,beta,d,x,r,s:real;
n,m,u,v:integer;
   begin
   write ('input a and alpha :  ');
   read (a);
   write ('  ');
   readln (alpha);
   write ('input b and beta :  ');
   read (b);
   write ('  ');
   readln (beta);
   write ('input d :  ');
   readln (d);
   x:=-0.25;
   n:=0;
   m:=99;
   hires;
   draw (0,0,0,199,1);
   draw (0,99,640,99,1);
   while x<1/4 do
      begin
      r:=-a*exp(-alpha*x*x)+b*exp(-beta*sqr(abs(x)-d));
      u:=trunc(1000*x)+250;
      v:=trunc(99-10*r);
      draw (n,m,u,v,1);
      n:=u;
      m:=v;
      x:=0.001+x;
      end;
   end.
```

Program "Unitcell" (TURBO-PASCAL) to calculate the scattering intensity of a model electron density profile:

```
program unitcell(input,output);
{  calculates the Fourier transform of the electron density  }
{  of the unitcell  }
   var
   pi,s,r,a,alpha,b,beta,c,d,i:real;
   u,v,x,y:integer;
   begin
        pi:=4*arctan(1);
        writeln ('pi = ',pi);
        s:=0;
        write ('r = ');
        readln (r);
        write ('a = ');
        readln (a);
        write ('alpha = ');
        readln (alpha);
        write ('b = ');
        readln (b);
        write ('beta = ');
        readln (beta);
        u:=0;
        v:=0;
        hires;
        draw(0,199,640,199,1);
        draw(0,0,0,199,1);
        while s<1/4 do
           begin
           c:=b/sqrt(beta)*2*cos(2*pi*s*r)*exp(-pi*pi*s*s/beta);
           d:=a/sqrt(alpha)*exp(-pi*pi*s*s/alpha);
           i:=2*sqr(c-d);
           x:=trunc(2000*s);
           y:=trunc(199-10*i);
           draw(u,v,x,y,1);
           u:=x;
           v:=y;
           s:=0.001+s;
           end;
        end.
```

Program "Interference function" (TURBO-PASCAL) to calculate the interference of a given number of bilayers:

```
program interference_function (input,output);
{  calculates the interference function for disorder of the  }
{  second kind (after Blaurock, 1982)  }
      var
      pi,s,r,z,o,q,l:real;
      n,m,u,v,x,y:integer;
      begin
         pi:=4*arctan(1);
         writeln ('pi = ',pi);
         s:=0;
         write ('input n:   ');
         readln (n);
         write ('input r and l: ');
         read (r);
         write ('  ');
         readln (l);
         write ('input z:   ');
         readln (z);
         writeln('');
         hires;
         draw(0,199,640,199,1);
         draw(0,0,0,199,1);
         u:=0;
         v:=0;
         while s<1/4 do
         begin
         o:=0;
         q:=0;
            for m:=1 to n-1 do
              begin
              o:=2*(n-m)*cos(2*pi*m*s*l)*exp(-m*z*s*s)+o;
              end;
            q:=(n+o);
            x:=trunc(2000*s);
            y:=trunc(199-q);
            draw(u,v,x,y,1);
            u:=x;
            v:=y;
            s:=0.001+s;
         end;
      end.
```

Program "Diffraction" (TURBO-PASCAL) to calculate the total scattering intensity of disordered multibilayers:

```
program diffraction (input,output);
{  calculates the diffracted X-ray intensity of the electron density  }
{  of the given unitcell, taking disorder into account  }
      var
      pi,s,r,a,alpha,b,beta,c,d,i,o,q,l,z:real;
      n,m,u,v,x,y:integer;
      begin
         pi:=4*arctan(1);
         writeln ('pi = ',pi);
         s:=0;
         write ('input n:  ');
         readln (n);
         write ('input r and l: ');
         read (r);
         write ('  ');
         readln (l);
         write ('input a and alpha: ');
         read (a);
         write ('  ');
         readln (alpha);
         write ('input b and beta: ');
         read (b);
         write ('  ');
         readln (beta);
         write ('input z:   ');
         readln (z);
         writeln ('');
         writeln('');
         hires;
         draw(0,199,640,199,1);
         draw(0,0,0,199,1);
         u:=0;
         v:=0;
         while s<1/4 do
            begin
            o:=0;
            q:=0;
            c:=b/sqrt(beta)*2*cos(2*pi*s*r)*exp(-pi*pi*s*s/beta);
            d:=a/sqrt(alpha)*exp(-pi*pi*s*s/alpha);
            i:=2*sqr(c-d);
            for m:=1 to n-1 do
            begin
            o:=2*(n-m)*cos(2*pi*m*s*l)*exp(-m*z*s*s)+o;
            end;
            q:=(n+o)*i;
            x:=trunc(2000*s);
            y:=trunc(199-q/20);
            draw(u,v,x,y,1);
            u:=x;
            v:=y;
            s:=0.001+s;
            end;
      end.
```